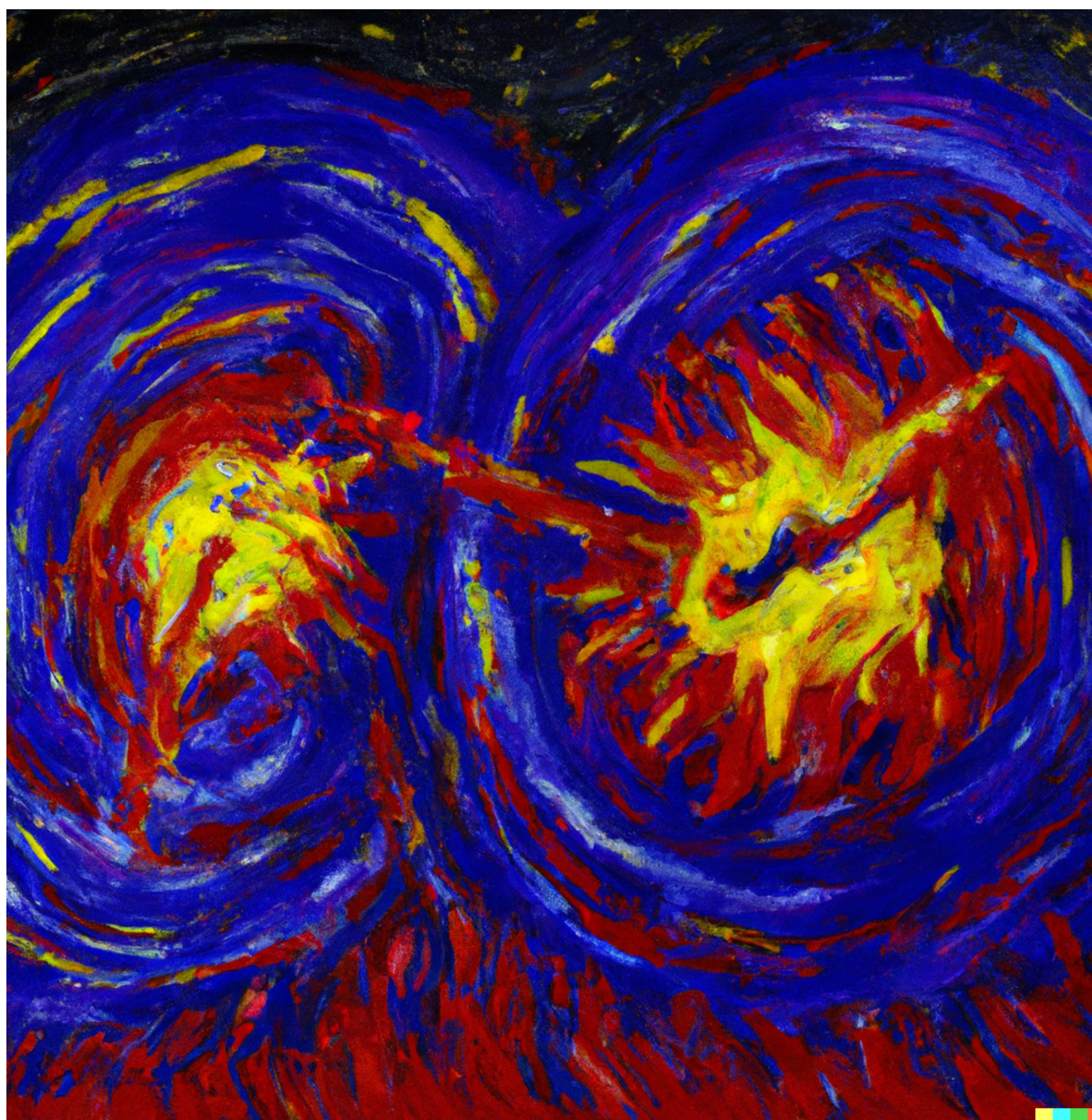
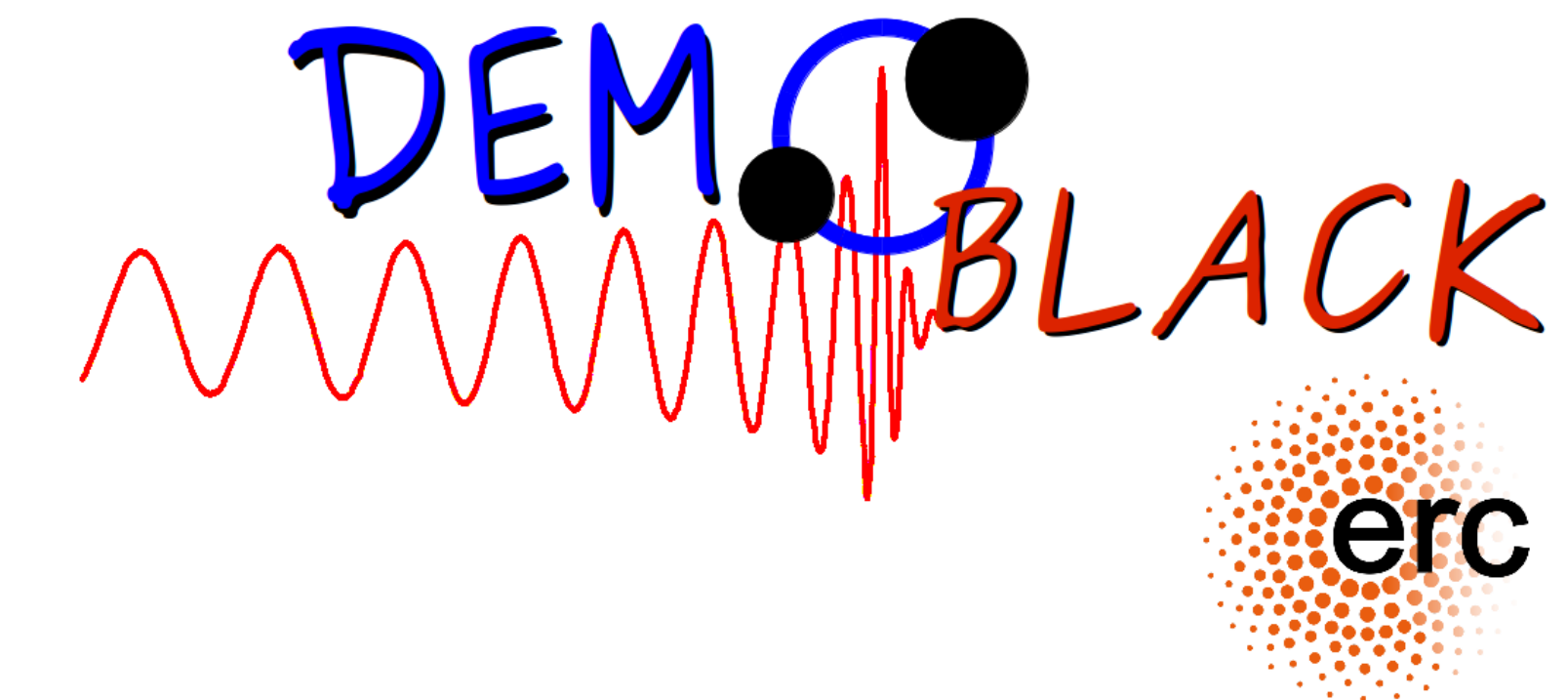


# Binary black hole mergers from Population III stars: uncertainties from star formation and binary star properties

Filippo Santoliquido



OpenAI. (2023). "Two merging stellar-mass black holes originating from population III stars in Kokoschka's artistic style " [Digital image]. Retrieved from <https://openai.com/dall-e/>

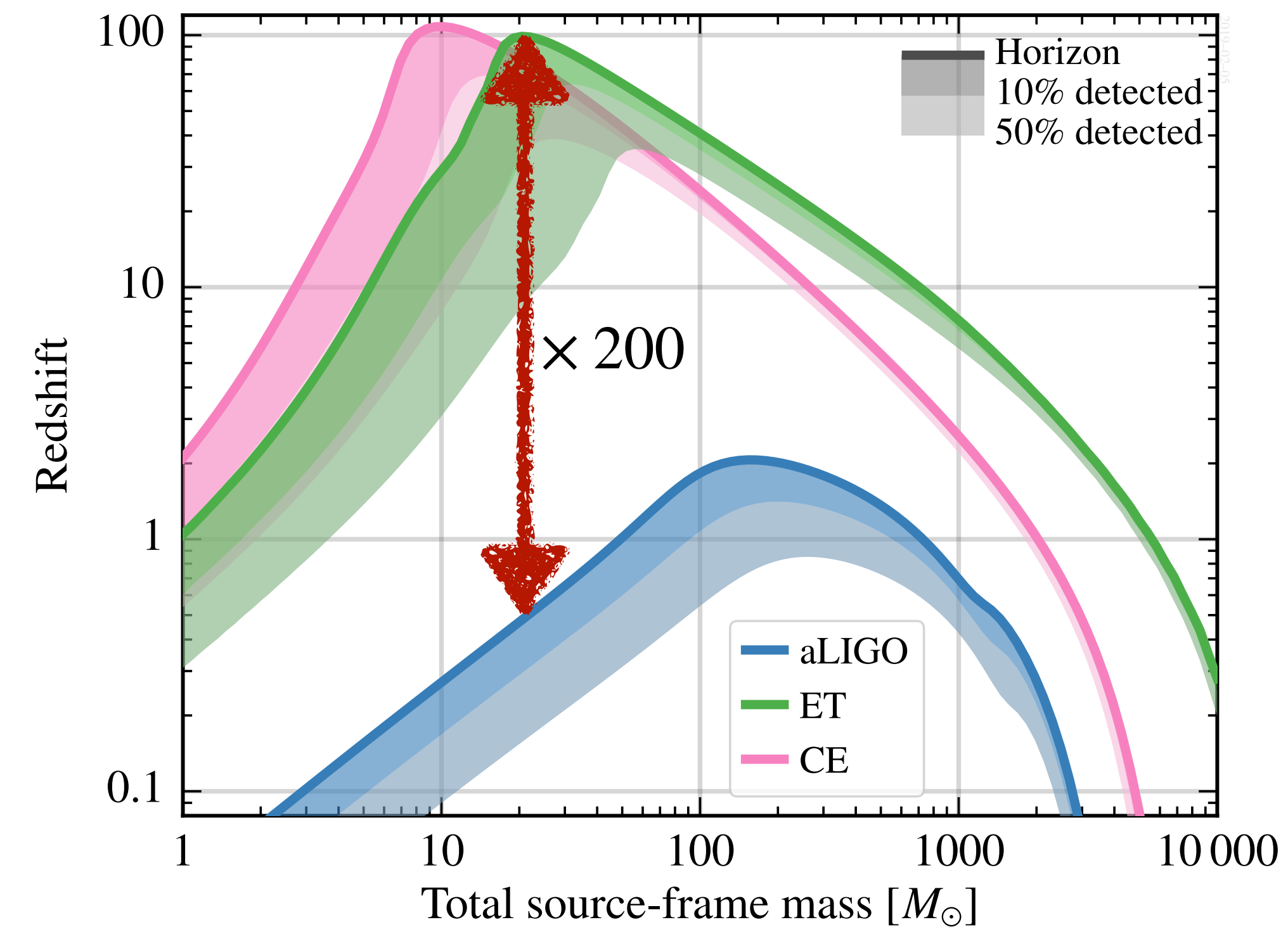


# Why Pop. III BBHs?

- **Einstein Telescope** will capture BBH mergers up to  $z \lesssim 100$  ([Maggiore et al. 2020](#); [Ng et al. 2021](#))
- **Population III** (Pop. III) binary stars likely produced the **first stellar-born BBH mergers** at high redshift ([Klessen & Glover 2023](#))
- Pop III. stars are the **first metal-free stars**. No **direct observations** thus large uncertainties ([Bromm & Larson 2004](#))

## 3G redshift horizon

<https://arxiv.org/pdf/2111.06990.pdf>



# what we decided to do...



Credit: ESO

[https://supernova.eso.org/exhibition/images/1120\\_pop3-CC/](https://supernova.eso.org/exhibition/images/1120_pop3-CC/)

- Large **parameter space exploration** on
  - **merger rate density** (aka *redshift distribution*) of Pop. III BBHs
  - **evolution of mass spectrum** with redshift
  - **expected detection rate of Einstein Telescope**

# Pop III. BBHs through population-synthesis

- We evolved a **large set** of Pop III. binary stars with our **most advanced population-synthesis code** SEVN
- **[Costa et al. 2023](#)** - [2303.15511](#) generated a brand new set of **Pop. III stellar evolution tracks**



is available at <https://gitlab.com/sevncodes/sevn>  
([lorio et al. 2022](#))

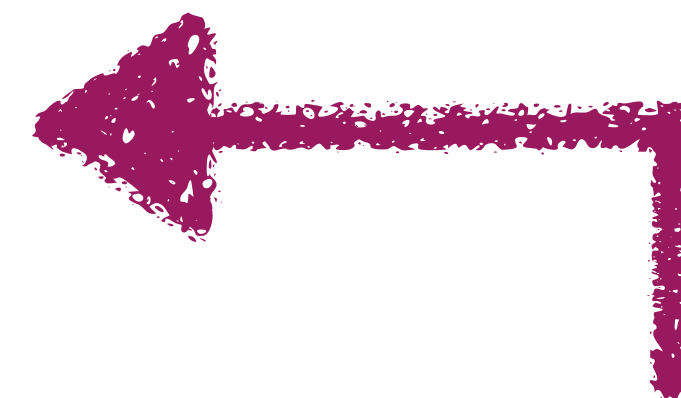
## Input VS Output

**Initial conditions:** IMF, period and eccentricity distribution, free parameters of binary evolution (e.g.  $\alpha$  of the common envelope)



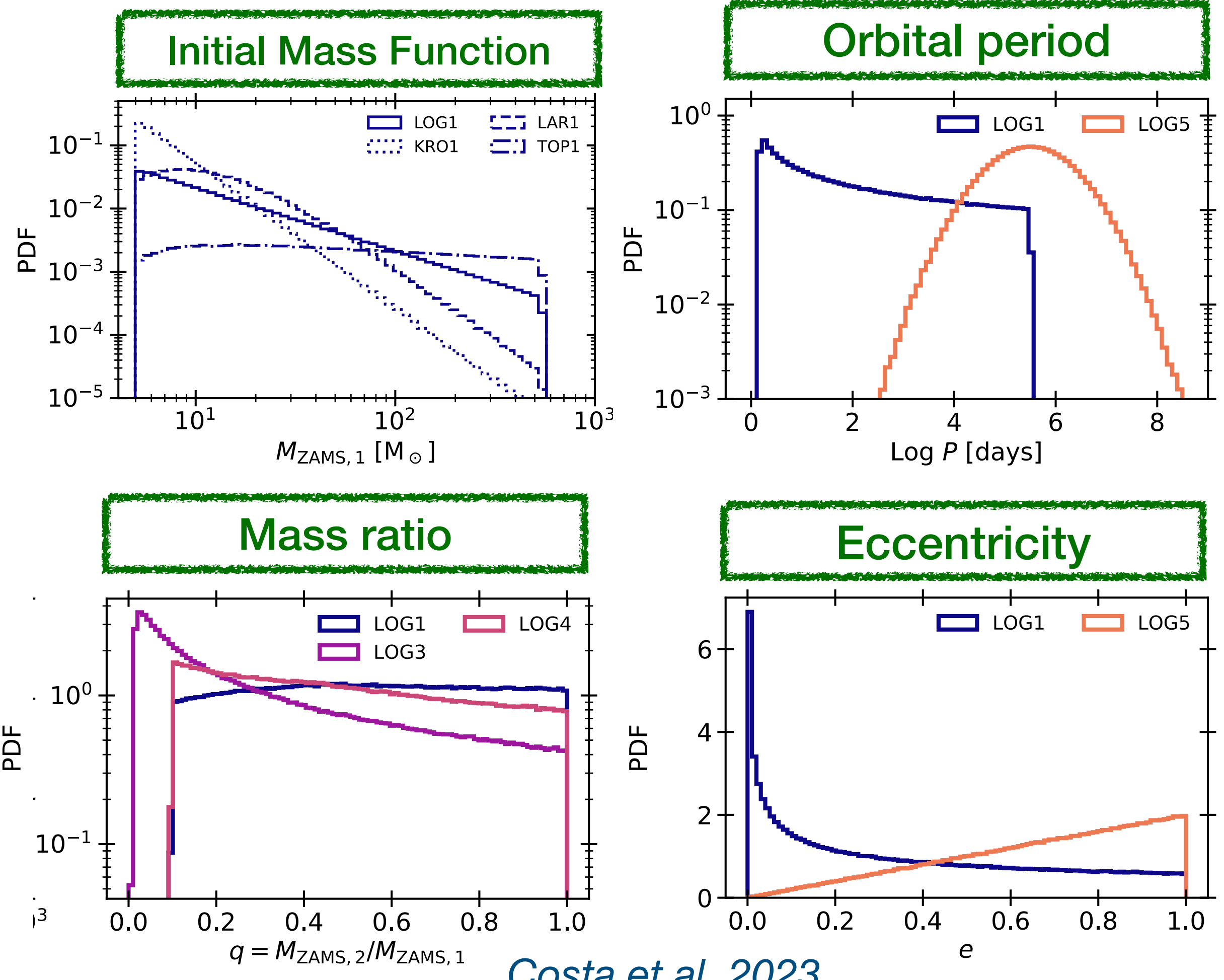
**Catalogs of merging BBHs,** defined by intrinsic parameters: primary mass, secondary mass, **delay time**, etc.

Santoliquido et al. 2020:  
<https://arxiv.org/pdf/2004.09533.pdf>

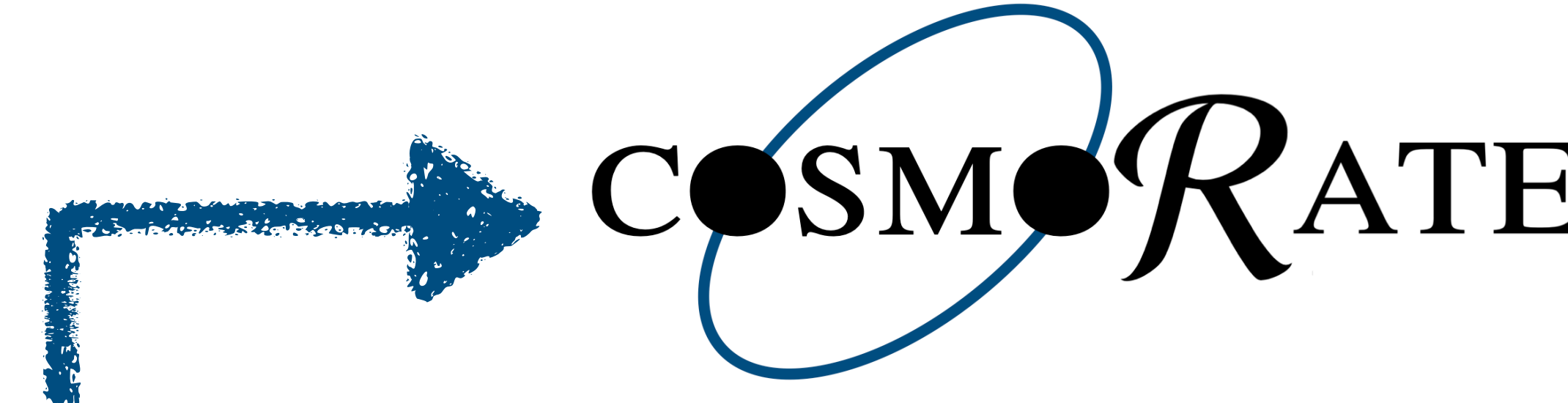


## large range of initial conditions:

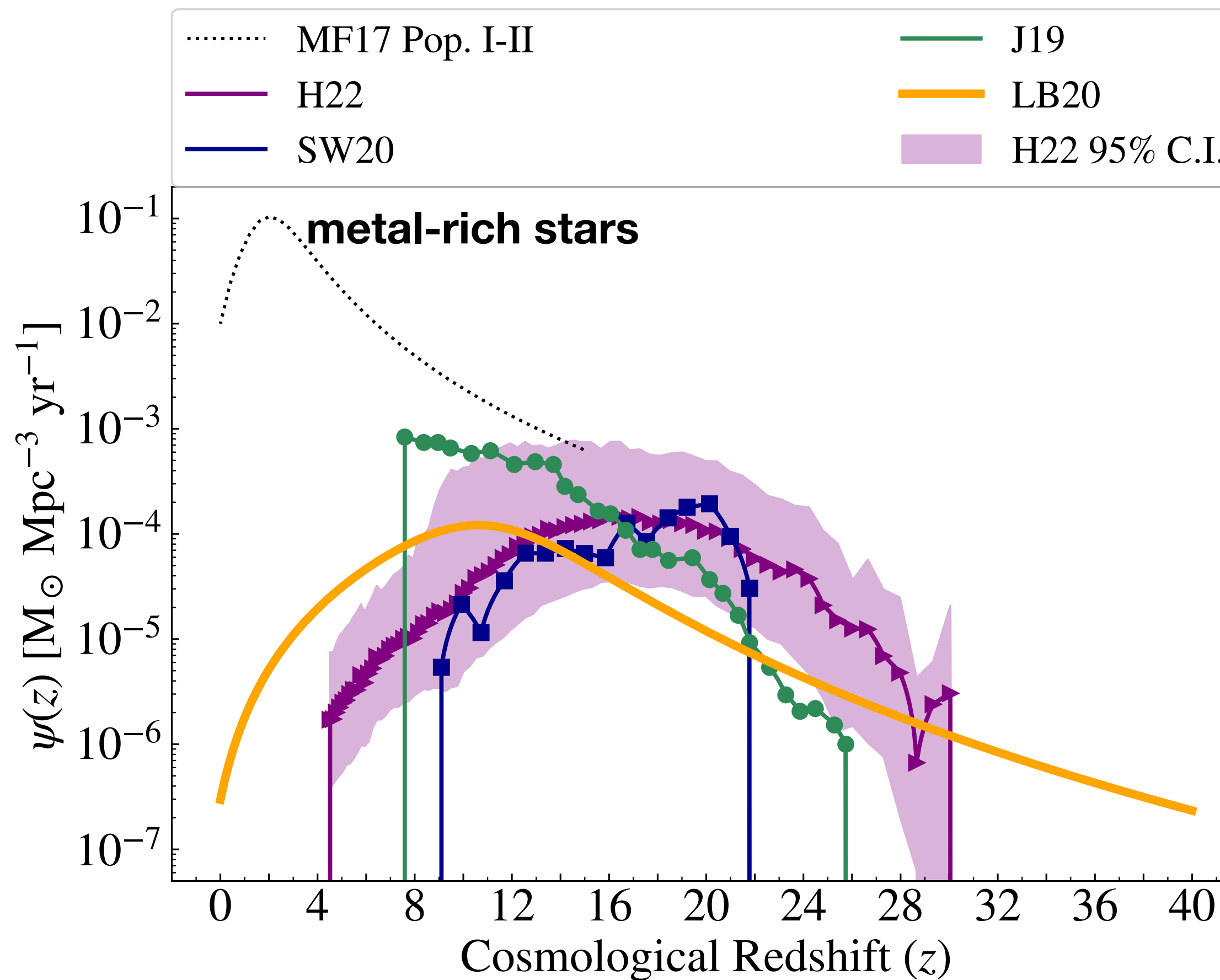
- 4 different initial mass functions
- 3 mass ratio distributions
- 2 orbital period distributions
- 2 eccentricity distributions
- **11 total combinations** (e.g. LOG1, KRO5, etc.)



[Costa et al. 2023](#)



is available at [https://gitlab.com/  
Filippo.santoliquido/  
cosmo\\_rate\\_public](https://gitlab.com/Filippo.santoliquido/cosmo_rate_public)



We considered four different estimates of  
Pop. III SFRD:

**H22** - [\*Hartwig et al. 2022\*](#)

**J19** - [\*Jaacks et al. 2019\*](#)

**LB20** - [\*Liu & Bromm 2020\*](#)

**SW20** - [\*Skinner & Wise 2020\*](#)

different assumptions on baryonic physics + cosmic variance

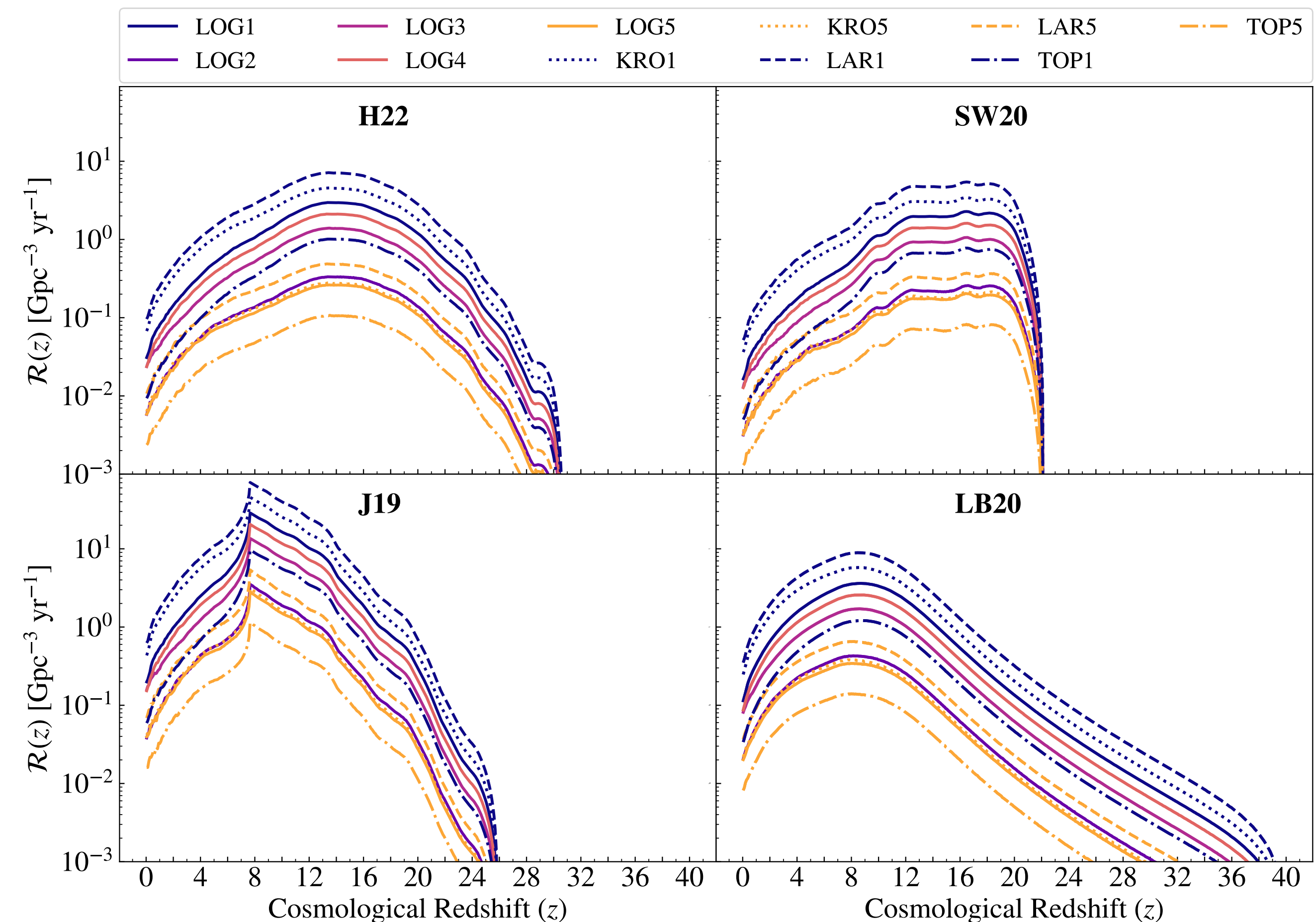
Santoliquido et al. 2023:

<https://arxiv.org/pdf/2303.15515.pdf>

# BBH merger rate density

- Uncertainties on the **initial conditions** impact by up to **two orders of magnitude**
- The **uncertainty on the star formation history** impacts both the **shape and the normalisation**
- The **peak** of the merger rate density **shifts** from  $z \sim 8$  (J19) up to  $z \sim 16$  (SW20)

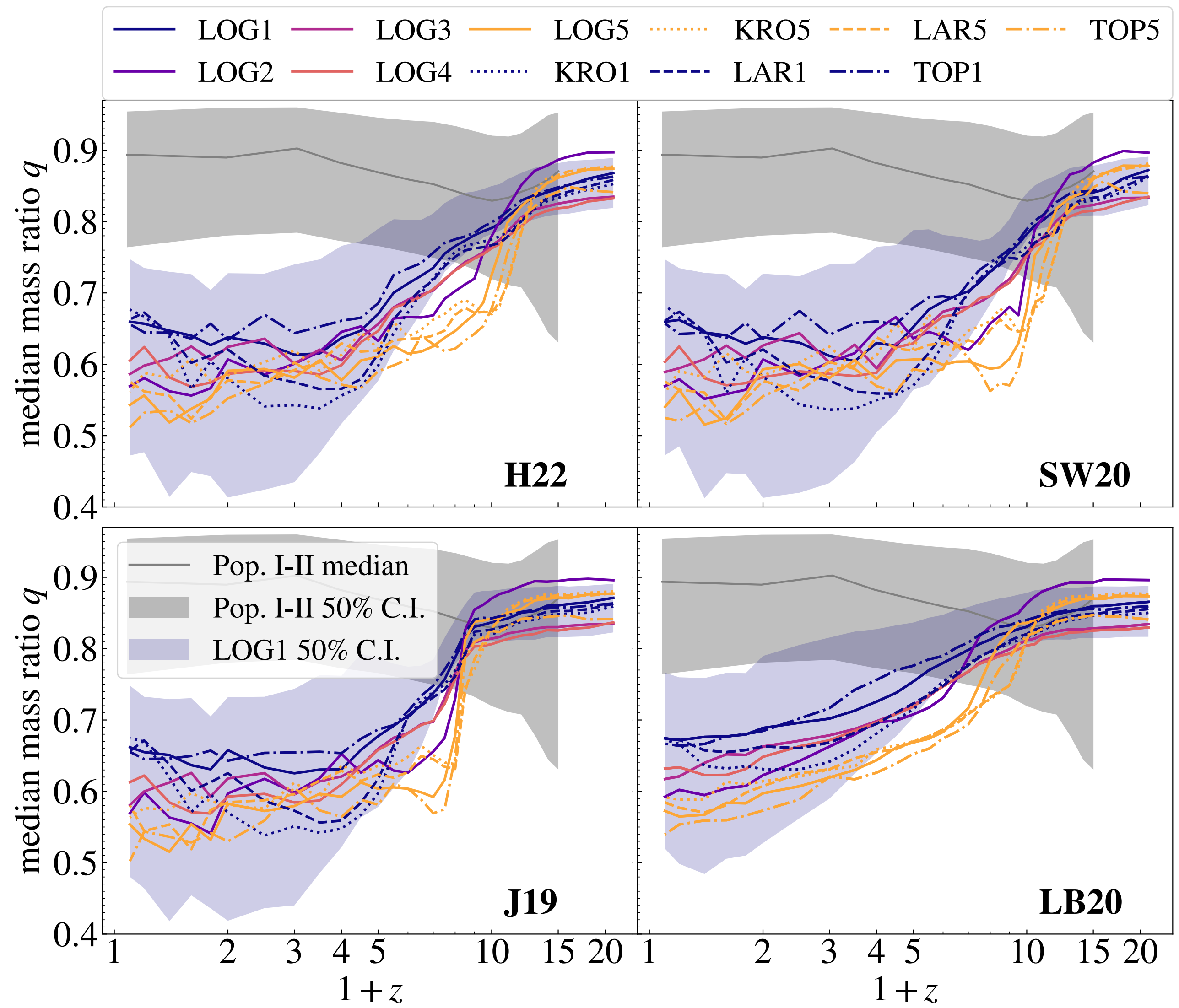
Santoliquido et al. 2023:  
<https://arxiv.org/pdf/2303.15515.pdf>



# mass ratio evolution

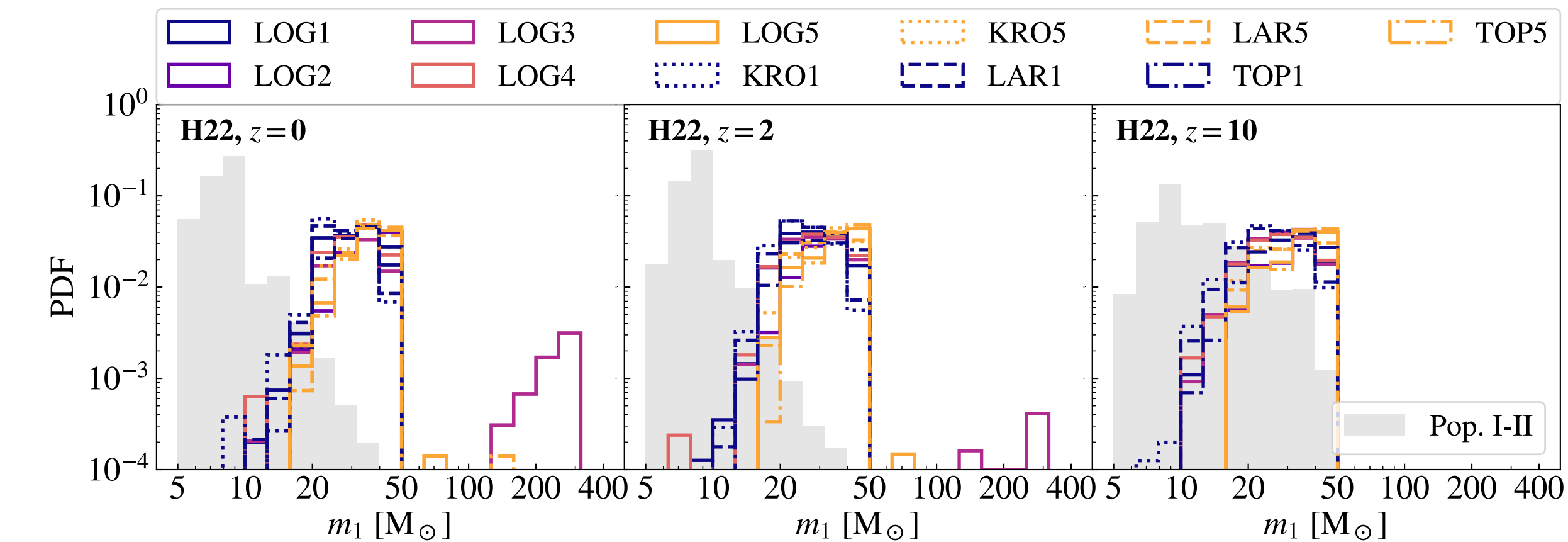
- The **mass ratio** of Pop. III BBHs **decreases with redshift**: from  $q \geq 0.9$  at  $z \sim 15$  to  $q \sim 0.5 - 0.7$  at  $z \leq 4$
- while mass ratio of **Pop. I-II** BBHs remains nearly **constant** (grey shaded area)
- These **features are shared** among different **initial conditions** and **SFRD** models
- Is this a **signature of Pop III. BBHs?**

Santoliquido et al. 2023:  
<https://arxiv.org/pdf/2303.15515.pdf>



# Primary mass

- At  $z = 0$ , Pop. I-II BBHs show a **main peak at 8 – 10 Msun**, similar to the ***main peak*** inferred from the LVK data ([Callister & Farr 2023](#))
- **primary BHs** born from Pop. III have a preference for  $m_1 \approx 30 - 35$  Msun, which is in the range of the ***secondary peak***



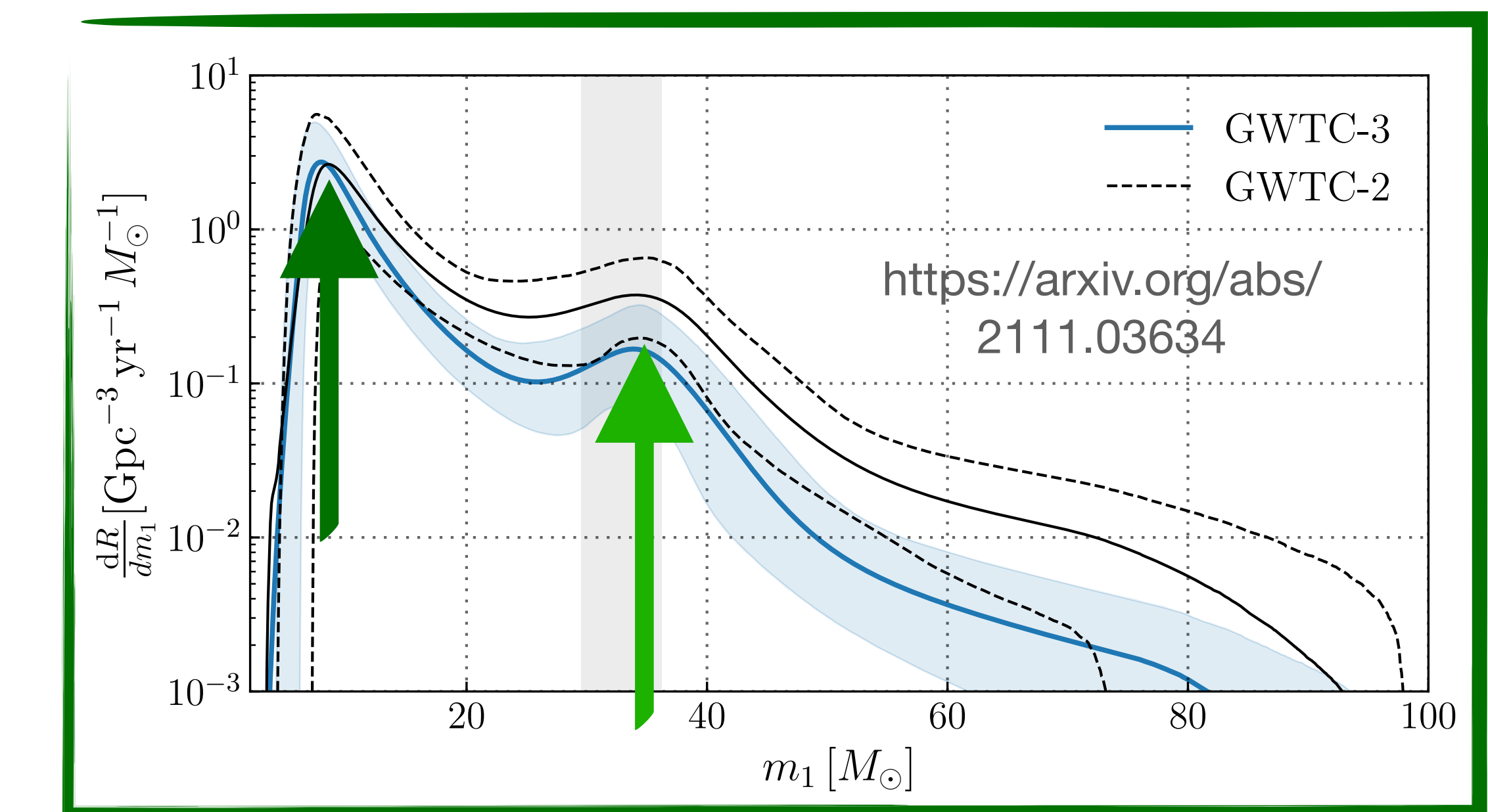
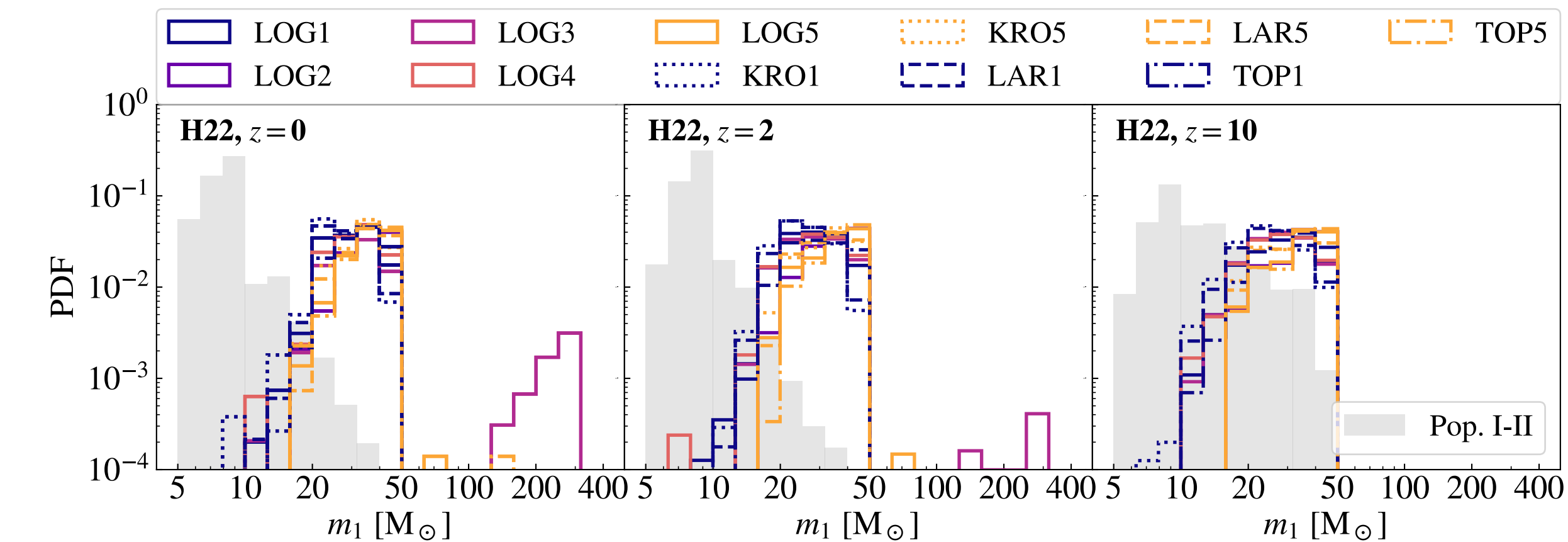
Santoliquido et al. 2023:

<https://arxiv.org/pdf/2303.15515.pdf>

# Primary mass

- At  $z = 0$ , Pop. I-II BBHs show a **main peak at  $8 - 10 \text{ Msun}$** , similar to the **main peak** inferred from the LVK data ([Callister & Farr 2023](#))
- **primary BHs born from Pop. III** have a preference for  $m_1 \approx 30 - 35 \text{ Msun}$ , which is in the range of the **secondary peak**

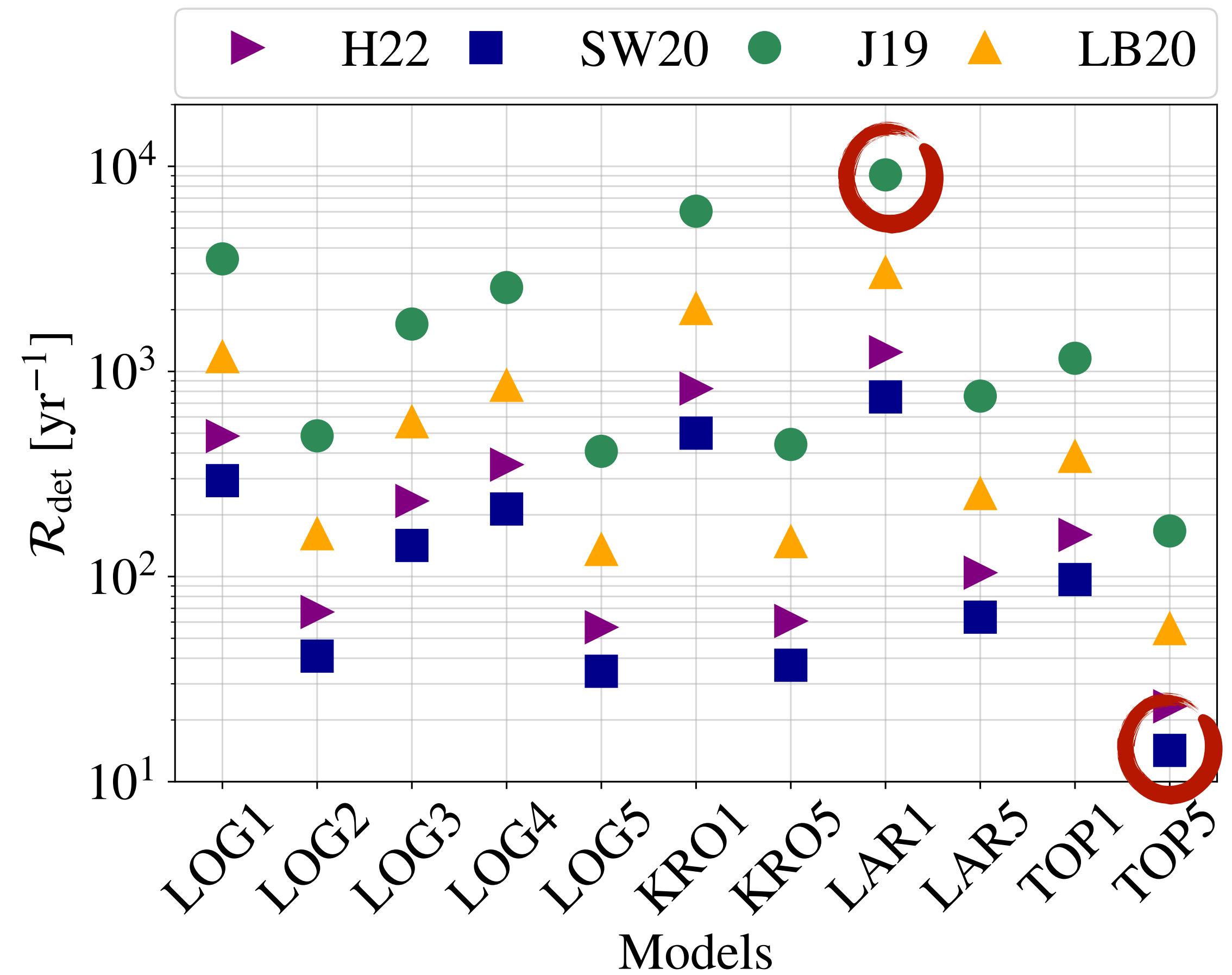
Santoliquido et al. 2023:  
<https://arxiv.org/pdf/2303.15515.pdf>



# detection rate

- Einstein Telescope will detect  $10 - 10^4$  Pop. III BBH mergers per year
- We expect between 23% and 73% of detections to occur at redshift  $z > 8$
- such high-redshift detections will be important to characterise the population of Pop. III BBHs.

Santoliquido et al. 2023:  
<https://arxiv.org/pdf/2303.15515.pdf>



# Conclusions

- We explored the **high-redshift sources** of astrophysical origins by making the first **large parameter exploration of Pop. III BBHs**
- This analysis serves the science case of **Einstein Telescope**
- The **assumed SFRD** affects both the **normalisation and shape** of the **BBHs merger rate density**
- Both the primary and secondary **BH** born from a **Pop. III** binary star tend to be **substantially massive**
- **Einstein Telescope** will detect  **$10 - 10^4$  Pop. III BBH mergers** per year, depending on the model

New manuscript!



Thank you

# Backup slides

# Intro

# from GWTC-*n* to the inferred merger rate density

90% credible intervals



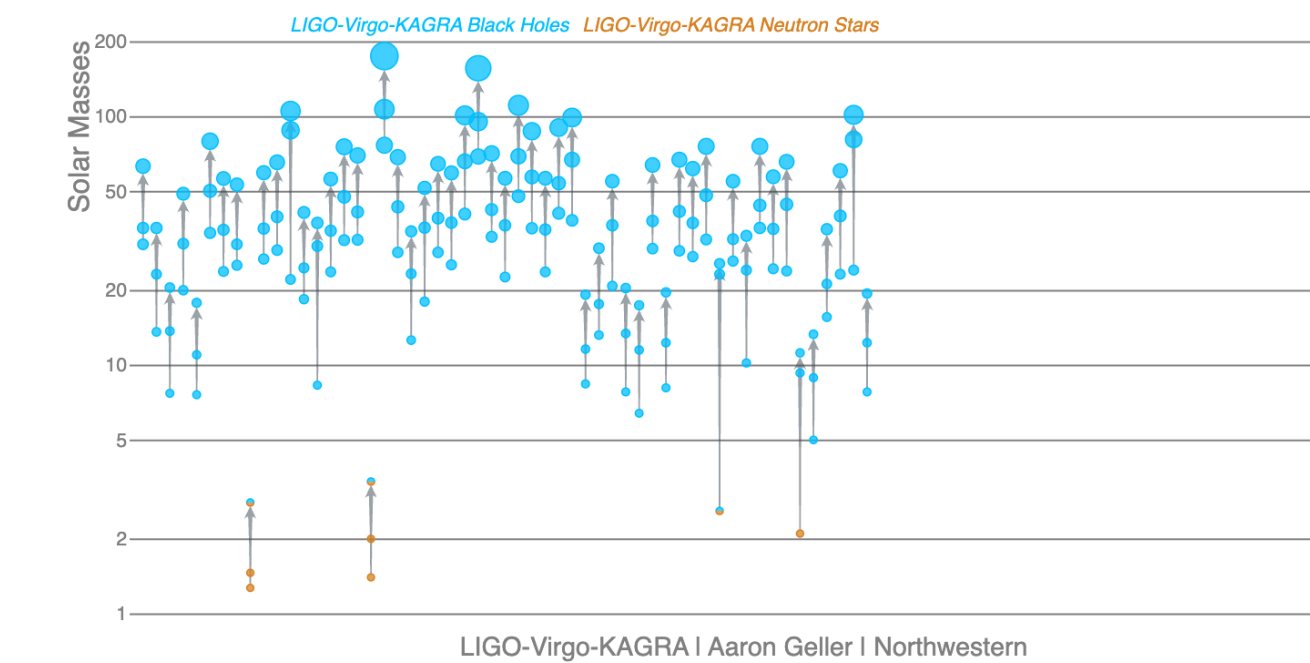
**GWTC-1**

$$\begin{aligned}\mathcal{R}_{\text{BBH}}^0 \\ \mathcal{R}_{\text{BHNS}}^0 \\ \mathcal{R}_{\text{BNS}}^0\end{aligned}$$

[24 - 140] Gpc<sup>-3</sup> yr<sup>-1</sup>

< 610 Gpc<sup>-3</sup> yr<sup>-1</sup>

[250 - 2810] Gpc<sup>-3</sup> yr<sup>-1</sup>

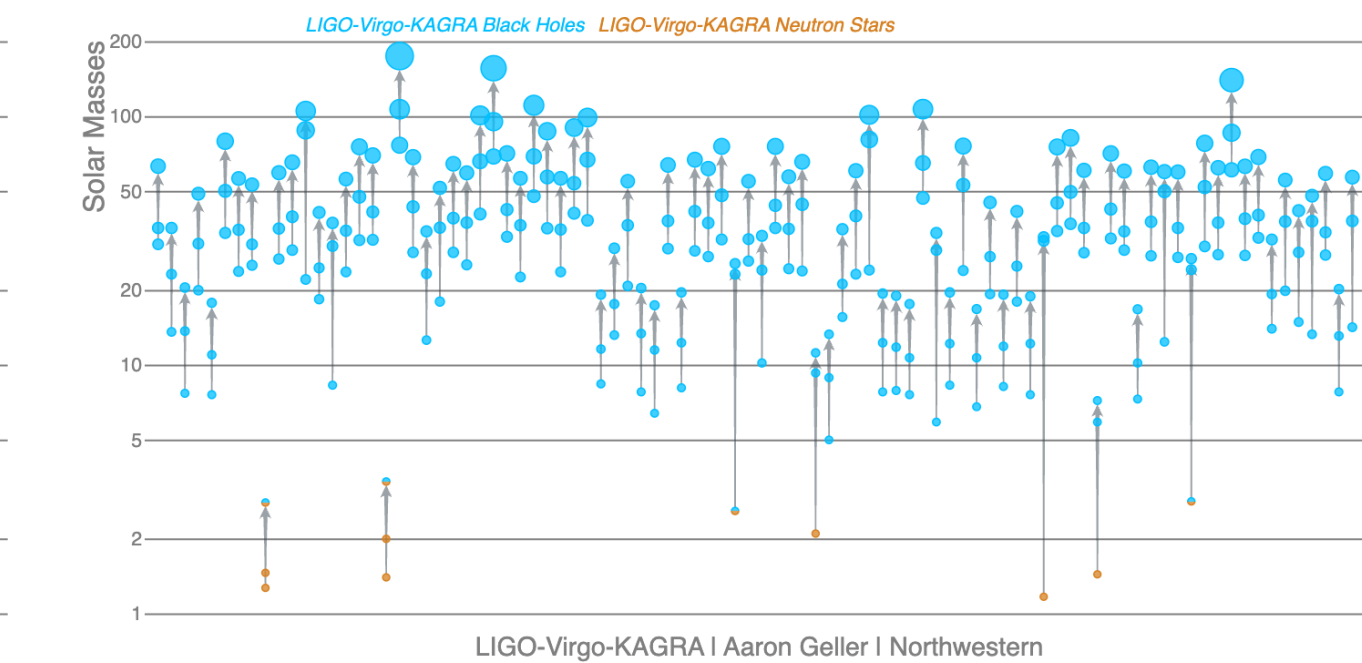


**GWTC-2**

[15 - 39] Gpc<sup>-3</sup> yr<sup>-1</sup>

< 610 Gpc<sup>-3</sup> yr<sup>-1</sup>

[80 - 810] Gpc<sup>-3</sup> yr<sup>-1</sup>



**GWTC-3**

[16 - 61] Gpc<sup>-3</sup> yr<sup>-1</sup>

[7.8 - 140] Gpc<sup>-3</sup> yr<sup>-1</sup>

[10 - 1700] Gpc<sup>-3</sup> yr<sup>-1</sup>

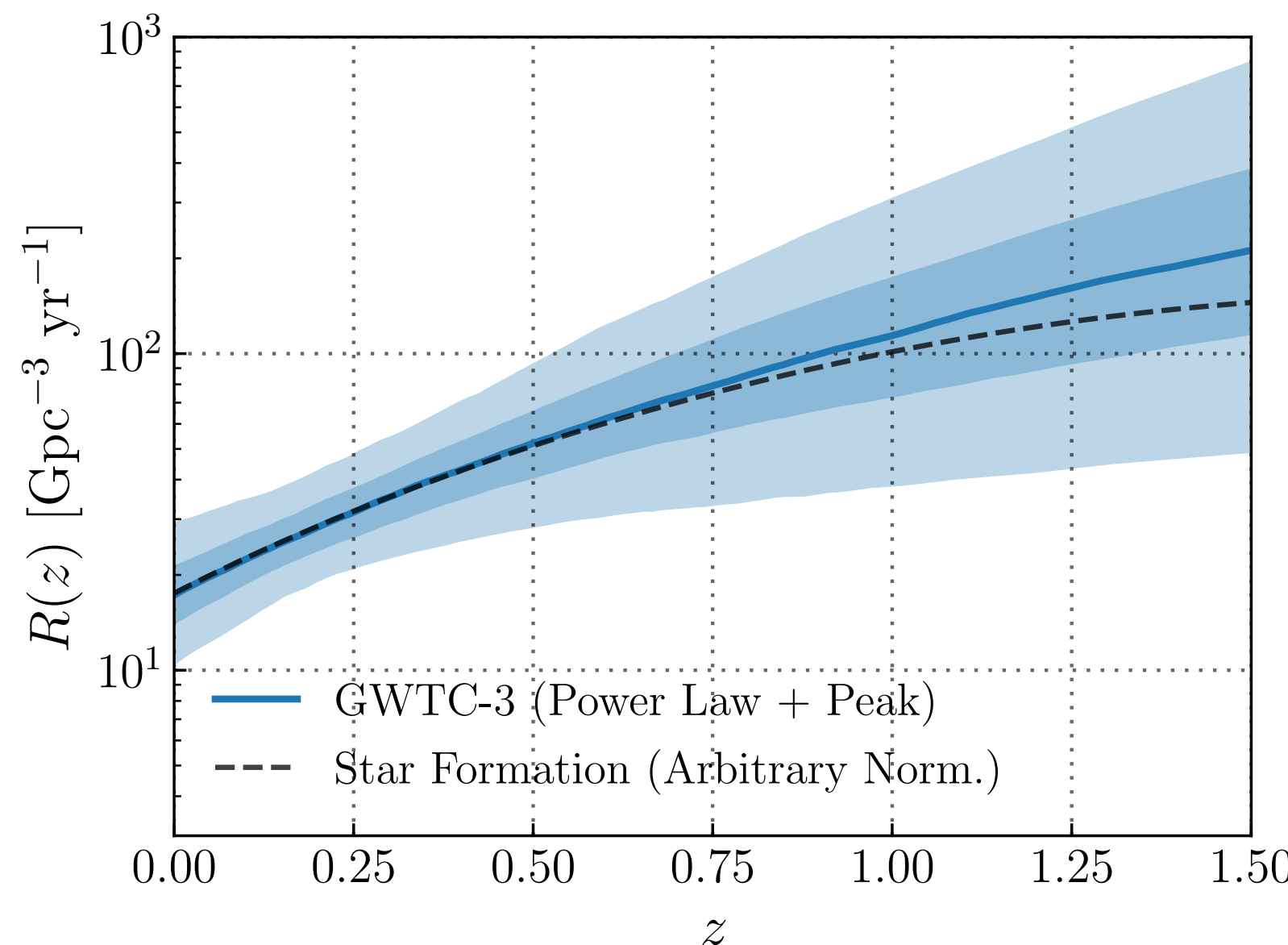
<https://arxiv.org/pdf/1811.12940.pdf>  
<https://arxiv.org/abs/1811.12907>  
<https://arxiv.org/pdf/2001.01761.pdf>

<https://arxiv.org/pdf/2010.14533.pdf>  
<https://arxiv.org/abs/1811.12907>

<https://arxiv.org/abs/2111.03634>

# redshift evolution of the merger rate density

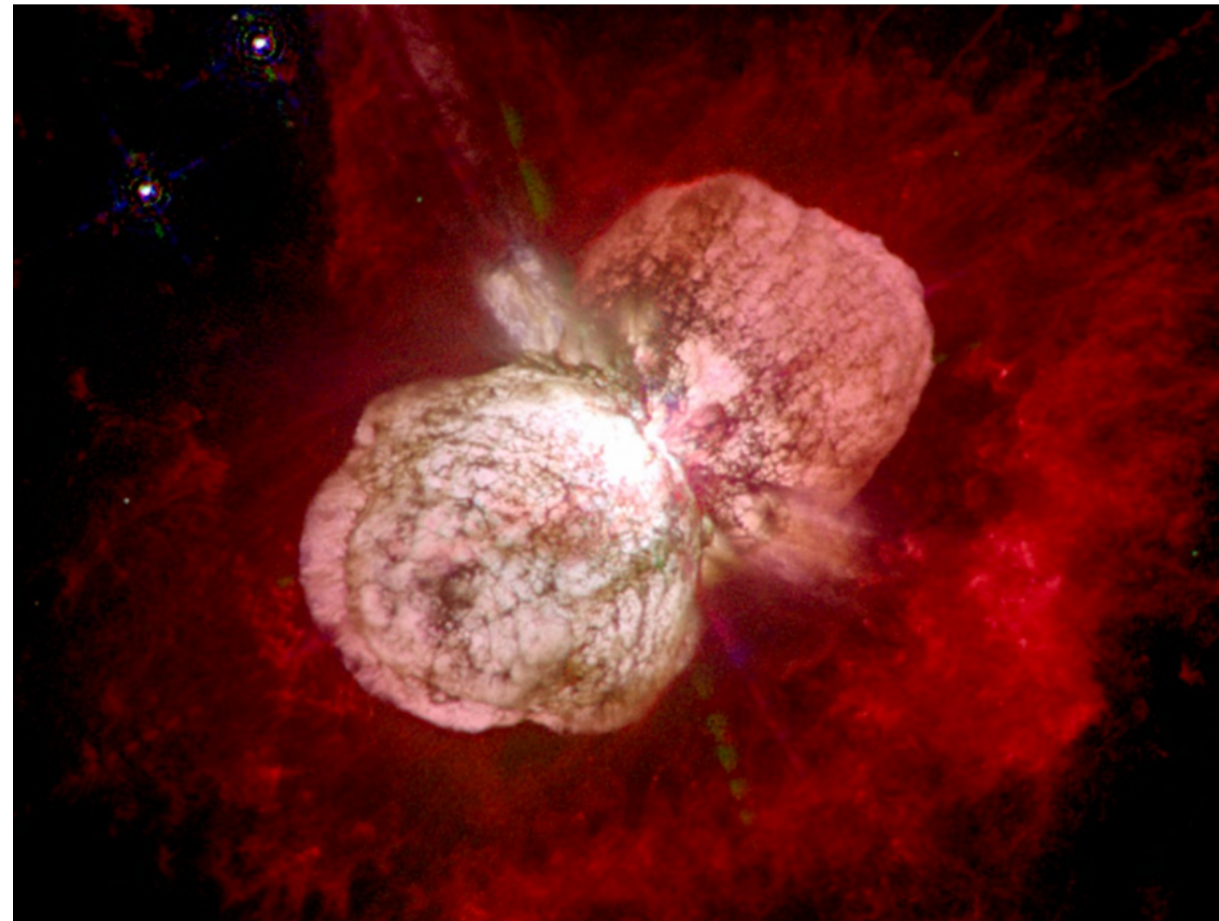
- high-mass **BBH**, LVK sensitivity allows for a **cosmologically significant reach**
- It is thus possible to infer the **evolution of merger rate density with redshift**
- LVK collaboration assumes the rate to evolve as:  $\mathcal{R}(z) = \mathcal{R}^0(1 + z)^\kappa$
- $\kappa > 0$  at 99% credibility



<https://arxiv.org/pdf/2111.03634.pdf>

# Population-synthesis

# how Pop. III BBH form?



Credit: NASA

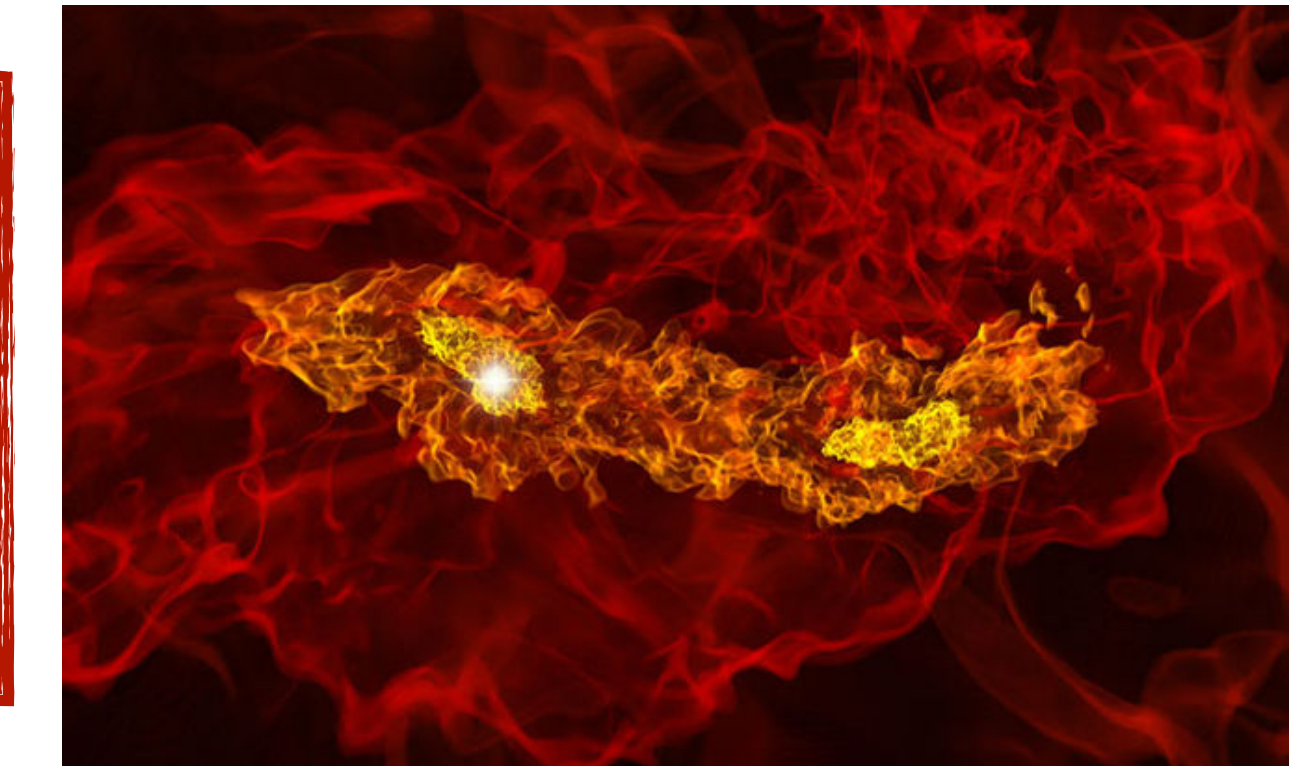
## Single stellar evolution:

Pop III. black holes are believed to form from massive stars at zero metallicity



## Isolated formation channel:

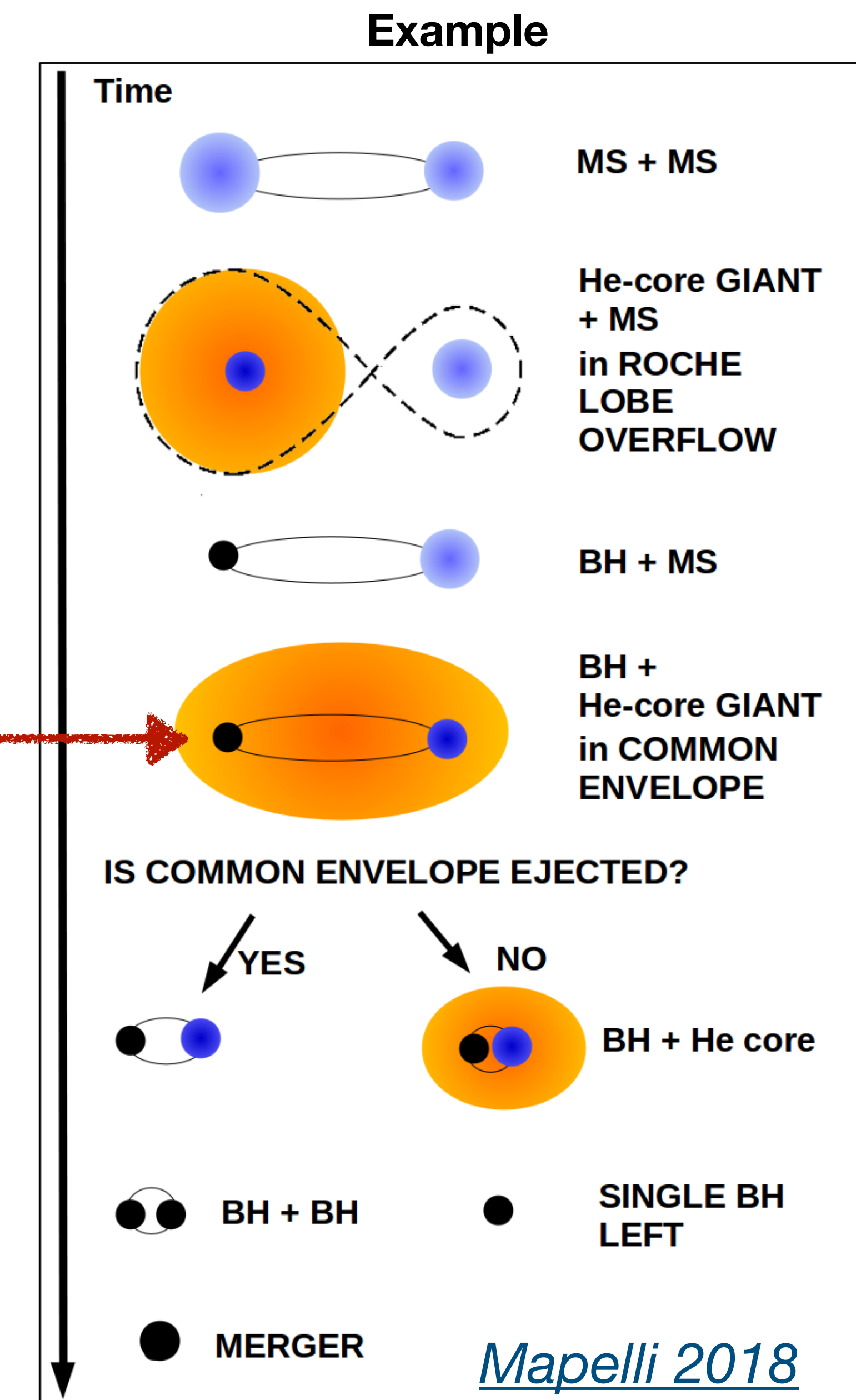
two stars in a binary system evolve into two compact objects that eventually merge within an Hubble time



Credit: NASA

# isolated formation channel: main physical processes

- **mass transfer** during Roche lobe overflow can be
  - *Stable* mass transfer (accretion efficiency  $f_{\text{MT}}$  [Mapelli 2018](#))
  - *Unstable* mass transfer leads to the **common envelope phase** ( $\alpha\lambda$ -formalism, [Webbink 1984](#)):
    - *basic idea:* the energy needed to **unbind the envelope** comes from the **loss of orbital energy** ( $\Delta E = E_{\text{env}}$ )
    - $\alpha$  measures the fraction of the removed orbital energy transferred to the envelope

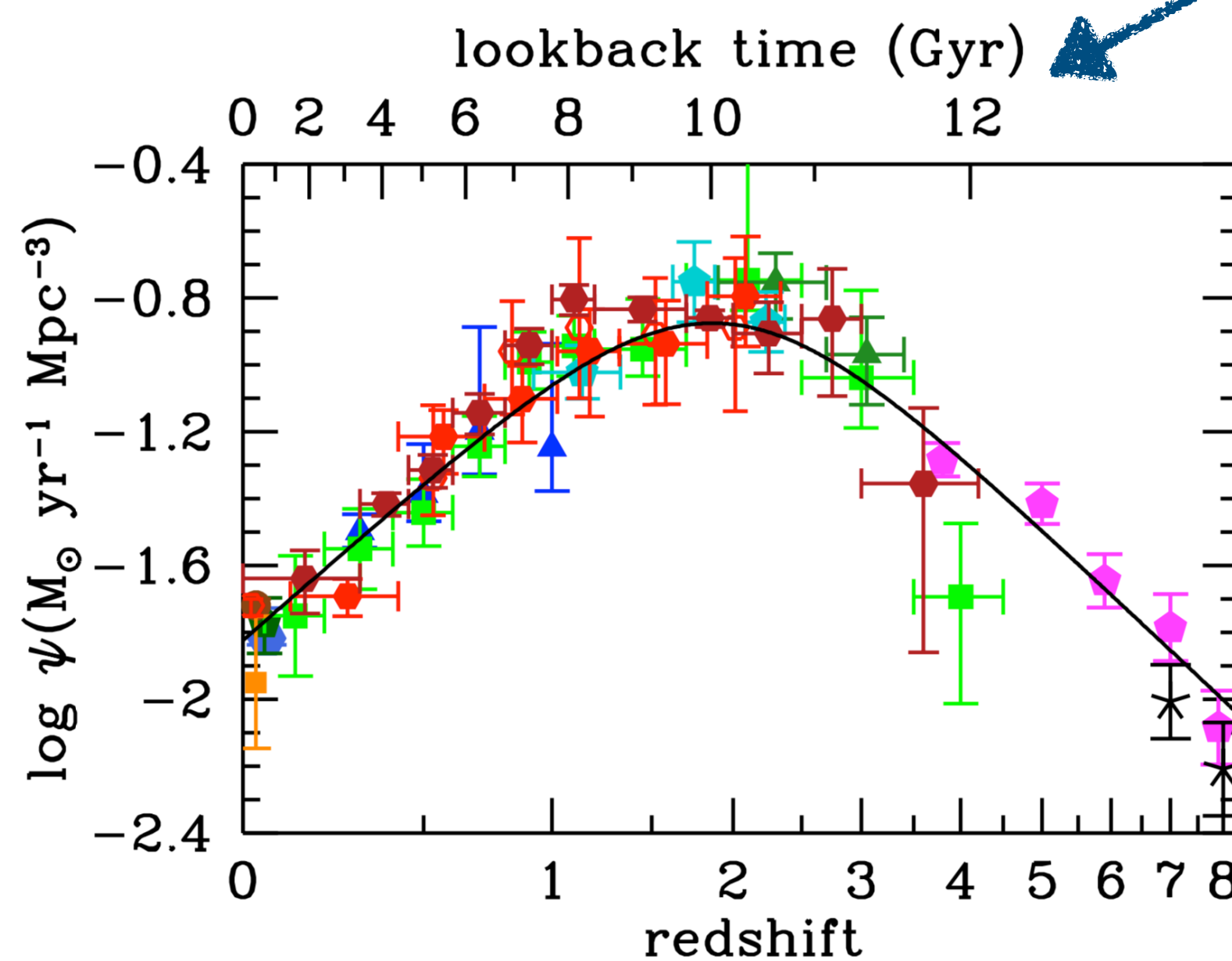


# $\alpha\lambda$ formalism for modelling the common envelope

- $\Delta E = \alpha(E_{b,f} - E_{b,i}) = \alpha \frac{Gm_{c1}m_{c2}}{2} \left( \frac{1}{a_f} - \frac{1}{a_i} \right)$  This is the orbital energy before and after the common envelope phase
- $E_{\text{env}} = \frac{G}{\lambda} \left[ \frac{m_{\text{env},1}m_1}{R_1} + \frac{m_{\text{env},2}m_2}{R_2} \right]$  This is the binding energy of the envelope
- By imposing  $\Delta E = E_{\text{env}}$ ,  $\frac{1}{a_f} = \frac{1}{\alpha\lambda} \frac{2}{m_{c1}m_{c2}} \left[ \frac{m_{\text{env},1}m_1}{R_1} + \frac{m_{\text{env},2}m_2}{R_2} \right] + \frac{1}{a_i}$
- Where  $\lambda$  is the parameter which measures the concentration of the envelope (the smaller  $\lambda$  is, the more concentrated is the envelope).
- The  $\alpha\lambda$  formalism is a simplified prescription. When  $\alpha > 1$ , we account for other sources of energy that make the envelope less bind, for instance recombination energy. Recent works (e.g. [Fragos et al. 2019](#)) suggest that  $\alpha > 1$  is necessary to reproduce the final orbital separation obtained with hydrodynamical simulations.

# COSMORATE

Santoliquido et al. 2020:  
<https://arxiv.org/pdf/2004.09533.pdf>



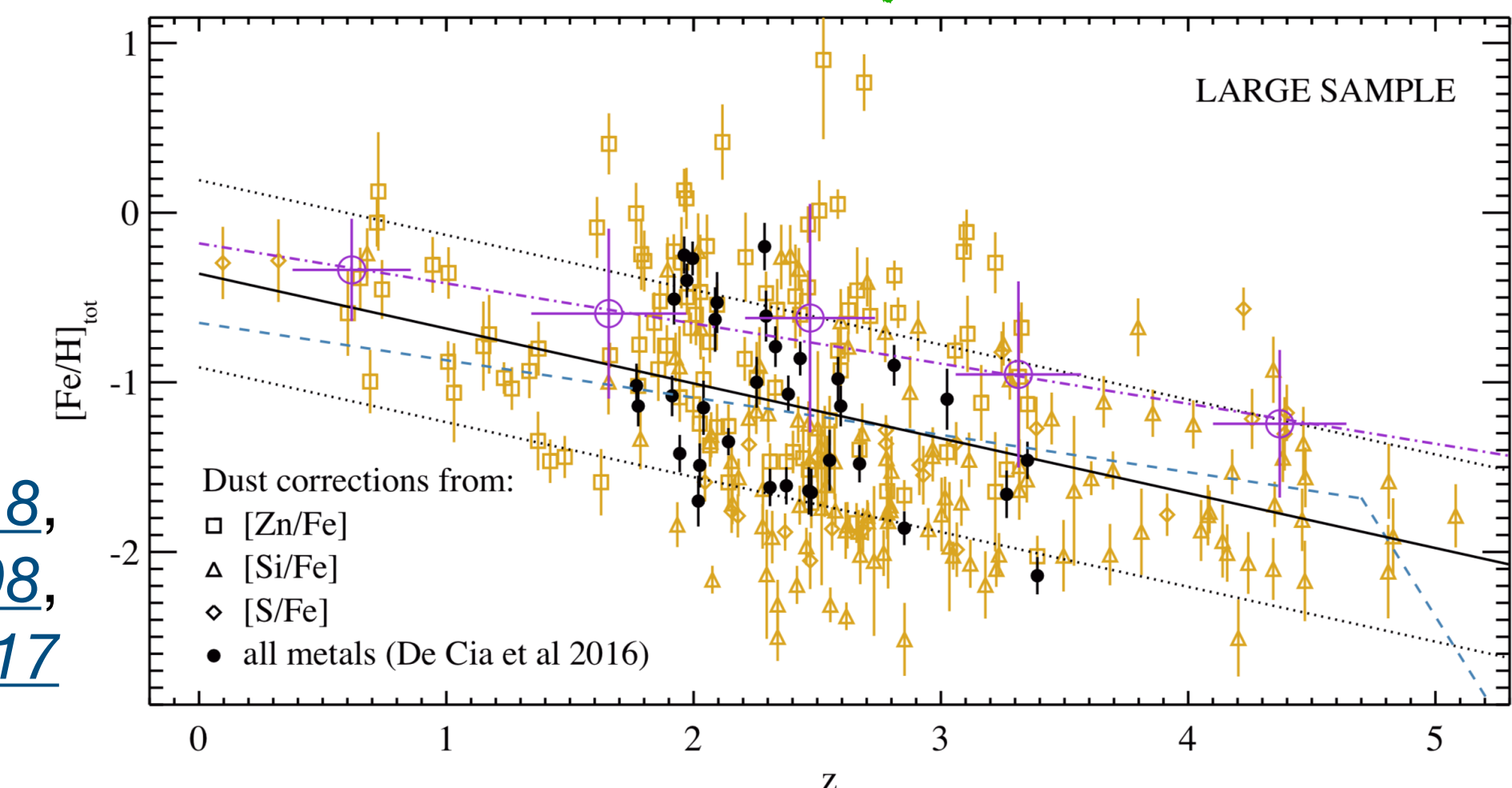
[Madau & Dickinson 2014](#), [Madau & Fragos 2017](#)

$$\mathcal{R}(z) = \int_{z_{\min}}^z \left[ \int_{Z_{\min}}^{Z_{\max}} \text{SFRD}(z', Z) \mathcal{F}(z', z, Z) dZ \right] \frac{dt(z')}{dz'} dz'$$

$$\text{SFRD}(z, Z) = \psi(z) p(Z|z)$$

$$p(Z|z) = \frac{1}{\sqrt{2\pi \sigma_Z^2}} \exp \left\{ - \frac{[\log(Z/Z_\odot) - \mu(z)]^2}{2\sigma_Z^2} \right\}$$

[De Cia et al. 2018](#),  
[Gallazzi et al. 2008](#),  
[Madau & Fragos 2017](#)



# Paper 4

# Initial conditions

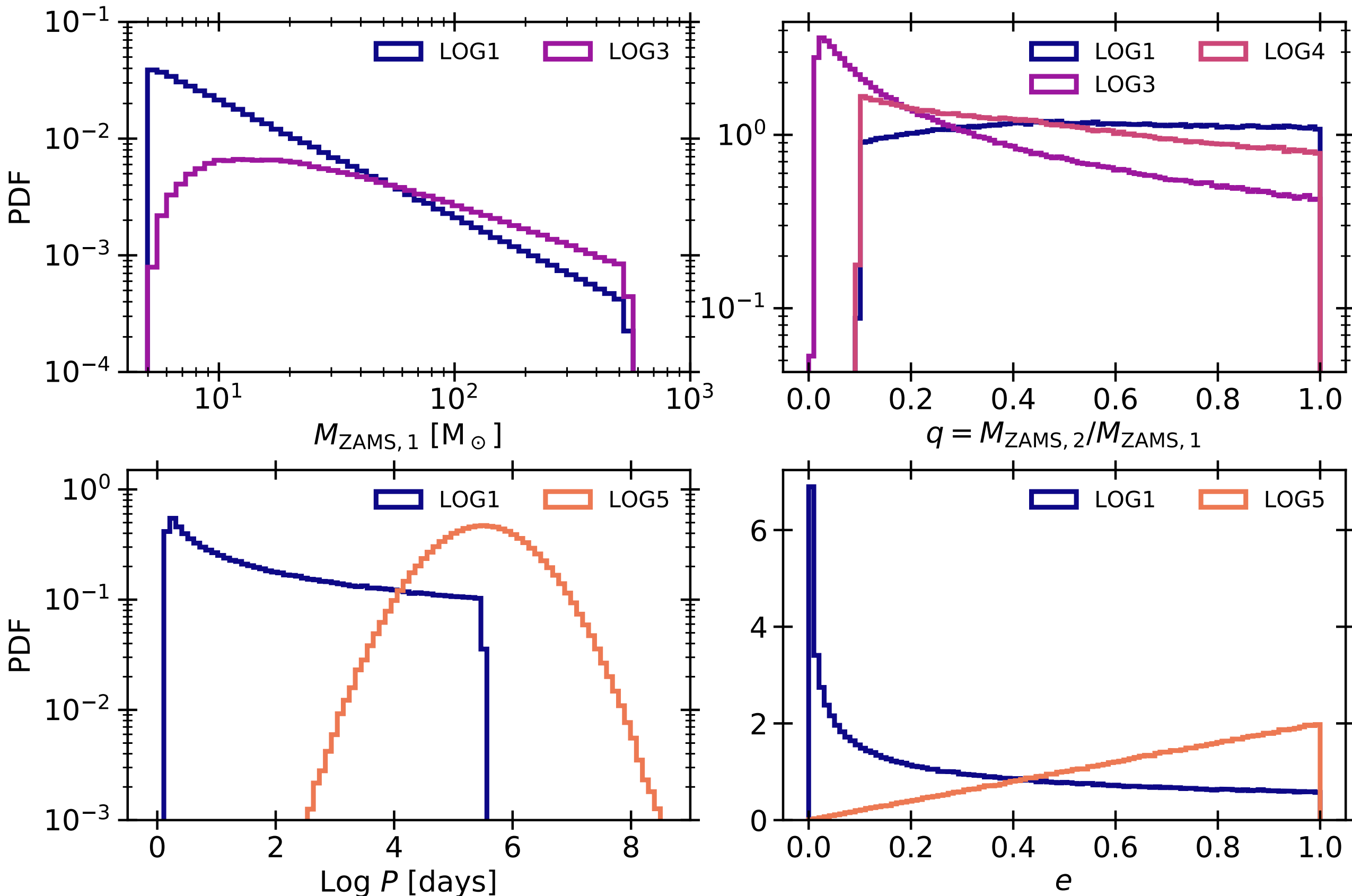
[Costa et al. 2023](#)

**Table 1.** Initial conditions.

Model	$M_{\text{ZAMS},1}$	$M_{\text{ZAMS}}$	$q$	$P$	$e$
LOG1	Flat in log	–	S12	S12	S12
LOG2	Flat in log	–	S12	SB13	Thermal
LOG3	–	Flat in log	Sorted	S12	S12
LOG4	Flat in log	–	SB13	S12	Thermal
LOG5	Flat in log	–	SB13	SB13	Thermal
KRO1	K01	–	S12	S12	S12
KRO5	K01	–	SB13	SB13	Thermal
LAR1	L98	–	S12	S12	S12
LAR5	L98	–	SB13	SB13	Thermal
TOP1	Top heavy	–	S12	S12	S12
TOP5	Top heavy	–	SB13	SB13	Thermal

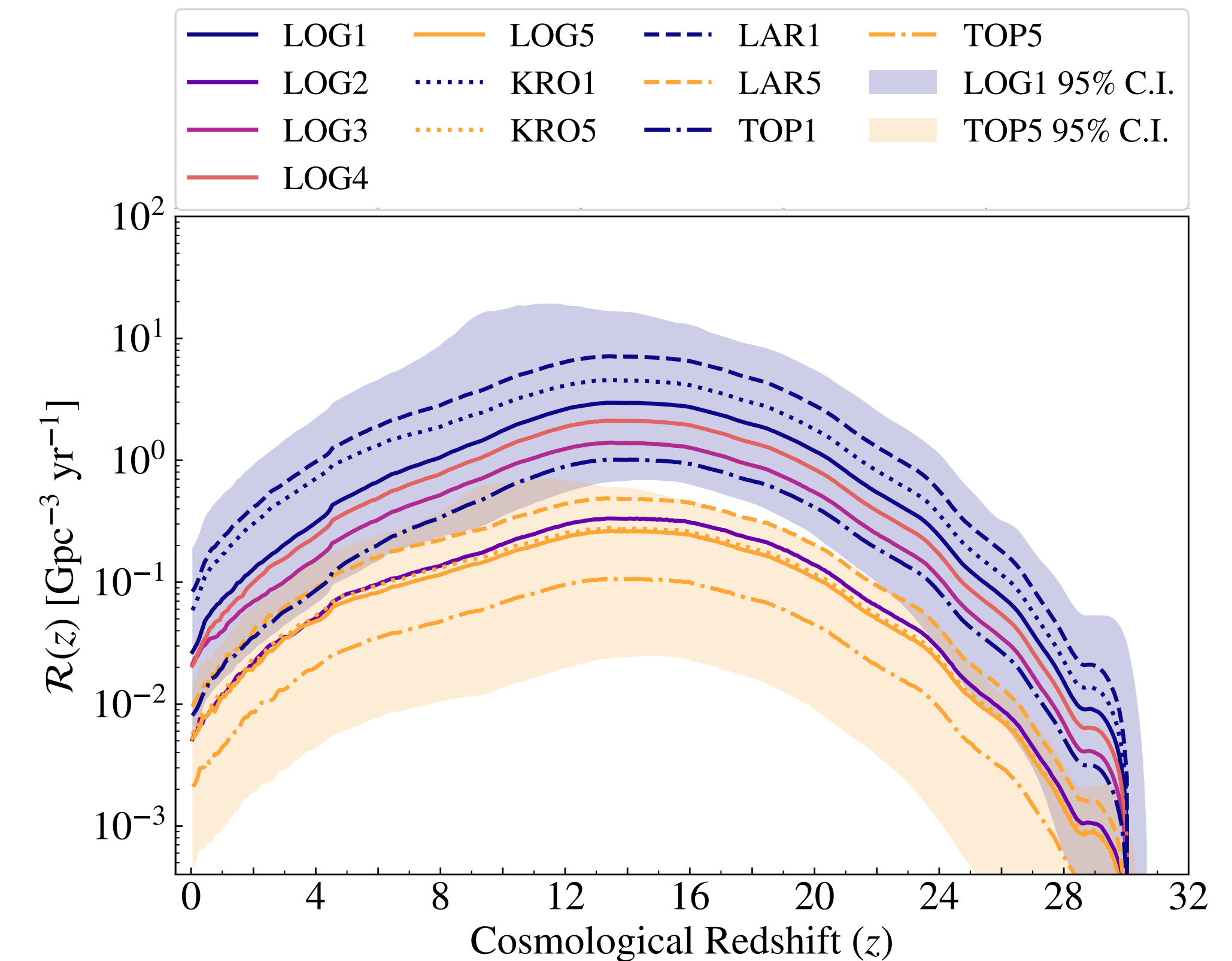
Column 1 reports the model name. Column 2 describes how we generate the ZAMS mass of the primary star (i.e., the most massive of the two members of the binary system). Column 3 describes how we generate the ZAMS mass of the overall stellar population (without differentiating between primary and secondary stars). We follow this procedure only for model LOG3 (see the text for details). Columns 4, 5, and 6 specify the distributions we used to generate the mass ratios  $q$ , the orbital periods  $P$  and the orbital eccentricity  $e$ . See Section 2.2 for a detailed description of these distributions.

**Santoliquido et al. 2023:**  
<https://arxiv.org/pdf/2303.15515.pdf>



**Figure 3.** Initial conditions for the models LOG1–5. From upper left to bottom right: ZAMS mass of the primary star  $M_{\text{ZAMS},1}$ , mass ratio  $q = M_{\text{ZAMS},2}/M_{\text{ZAMS},1}$ , initial orbital period  $P$ , and initial orbital eccentricity  $e$ . In the upper-left panel, we do not show models LOG2, LOG4 and LOG5 for simplicity, because they follow the same distribution as LOG1 (i.e.,  $M_{\text{ZAMS},1}$  is sampled from a flat-in-log distribution), while in model LOG3 we sample the entire stellar population (i.e., both primary and secondary stars) from a flat-in-log distribution. In the upper-right panel ( $q$ ), model LOG2 follows the same distribution as LOG1 (S12), while model LOG5 follows the same distribution as LOG4 (SB13). In the lower-left panel ( $P$ ), models LOG3 and LOG4 follow the same distribution as LOG1 (S12), while models LOG2 and LOG5 are sampled from SB13. Finally, in the lower-right panel ( $e$ ), models LOG1 and LOG3 follow S12, while the other models adopt a thermal distribution (we show only LOG5 for simplicity). Table 1 describes the models in detail.

- With A-SL0TH, it is possible to quantify the uncertainties in the SFRD that arise from unconstrained input parameters of the semi-analytic model (such as star formation efficiency or Pop. III IMF).
- We propagate these uncertainties in the merger rate density. Here, we show the 95% credible interval



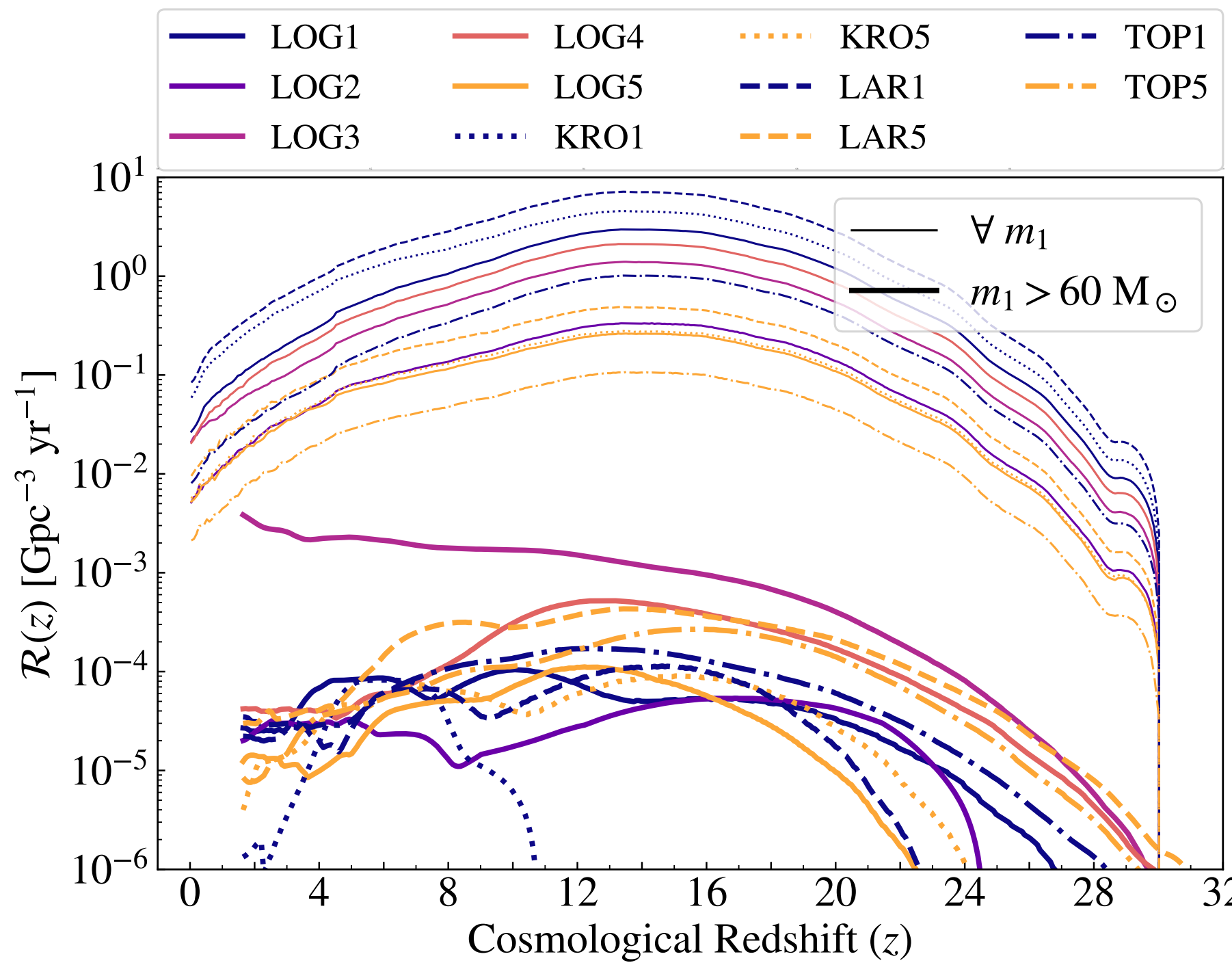
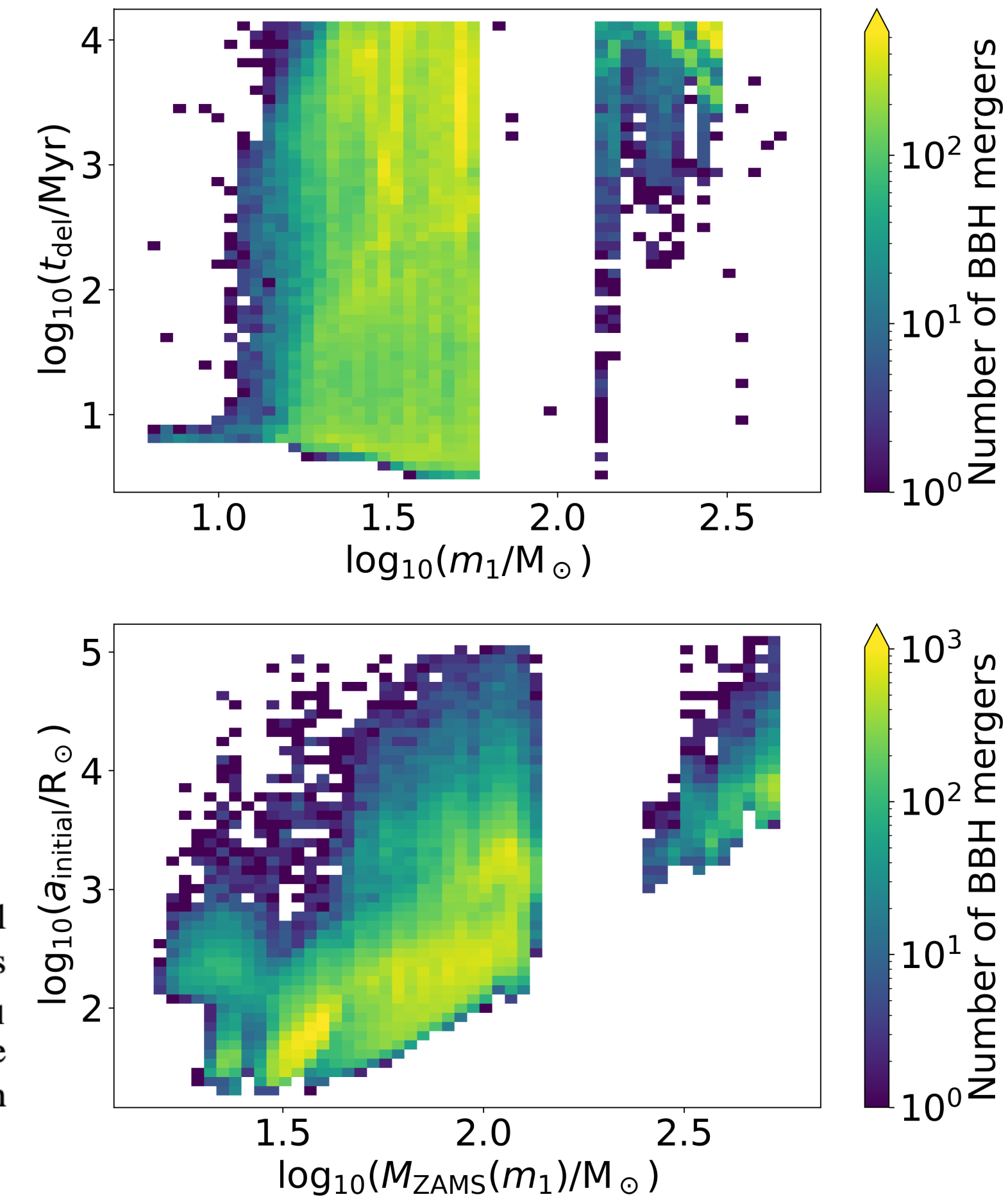
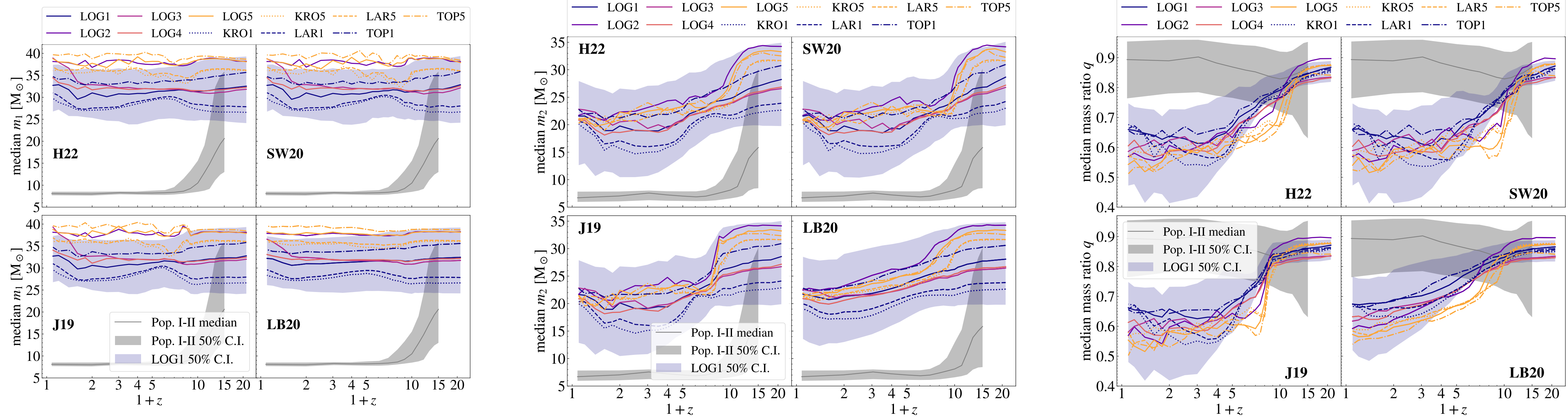


**Figure 15.** Properties of Pop. III BBH mergers and their progenitors in model LOG3. Upper panel: delay time  $t_{\text{del}}$  as a function of the primary BH mass  $m_1$ . Lower panel: initial semi-major axis of the progenitor binary star  $a_{\text{initial}}$  versus ZAMS mass of the progenitor of the primary BH  $M_{\text{ZAMS}}(m_1)$ . These data come directly from the SEVN catalogues and are not convolved with redshift evolution.

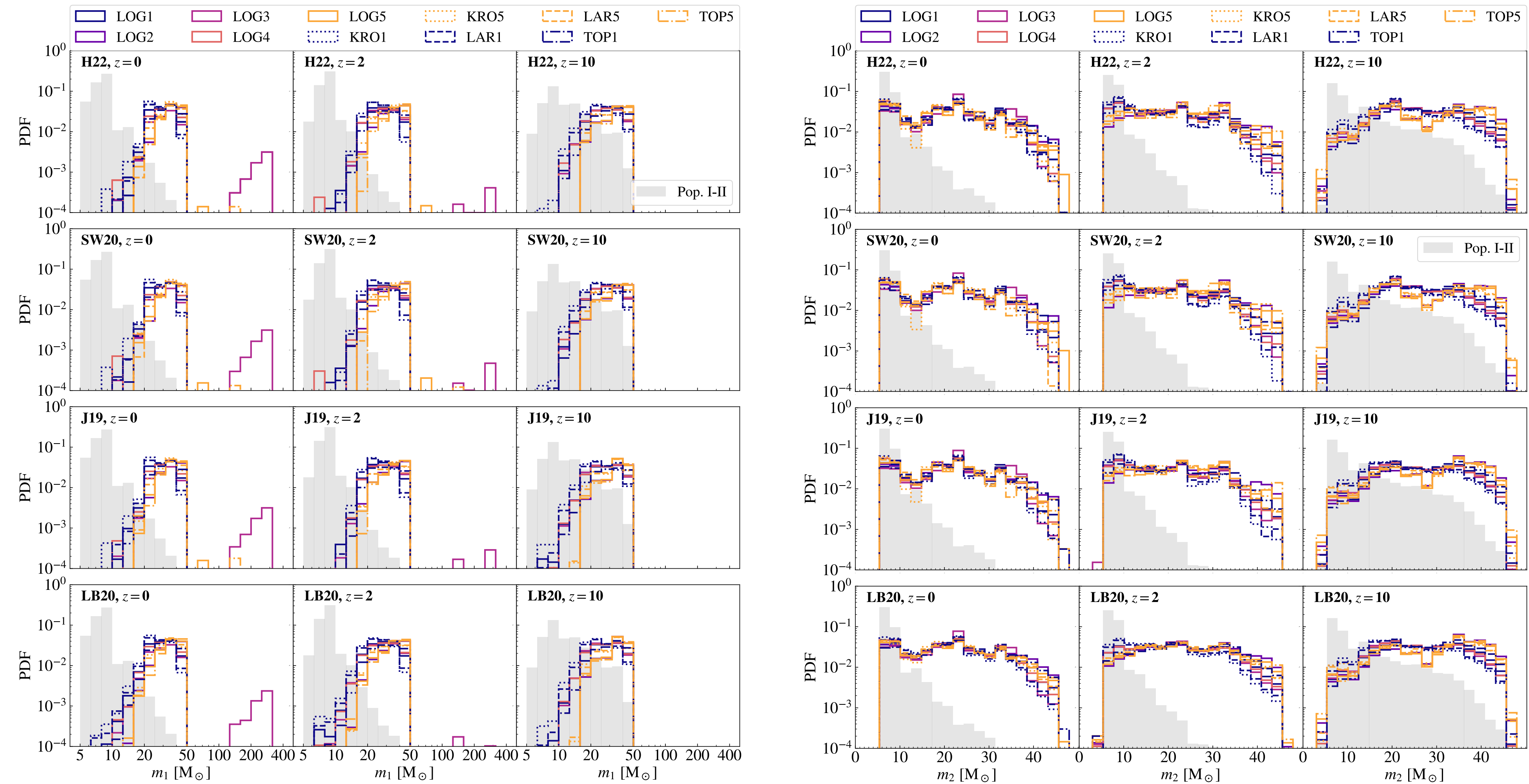
**Figure 16.** The thick lines show the merger rate density evolution of Pop. III BBHs with primary BH mass  $m_1 > 60 M_\odot$ . For comparison, the thin lines show the total merger rate density evolution of Pop. III BBHs (for any value of  $m_1$ ). For all the models in this Figure, we use the Pop. III star SFRD from H22 (Figure 1). The colours and line types refer to different initial orbital parameters (Table 1).



# Pop. III BBHs: mass evolution



# Pop. III BBHs: mass evolution



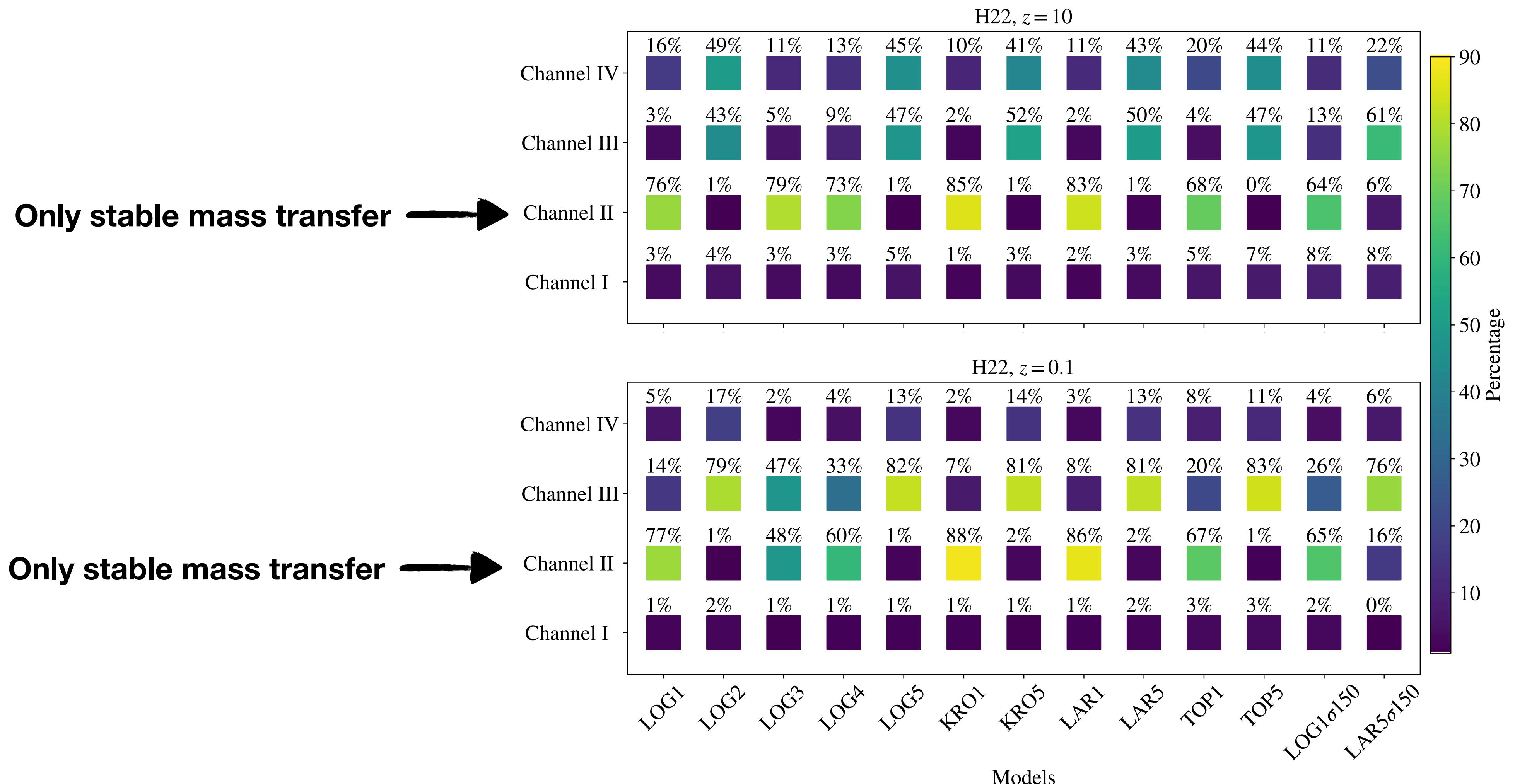


**Figure 10.** Percentage distribution of formation channels for all the models adopted in this work. Upper (lower) panel: Pop. III BBHs that merge at  $z = 10$  ( $z = 0.1$ ). Channel I includes all the systems that undergo a stable mass transfer before the first BH forms, and later evolve through at least one common-envelope phase. Channel II encompasses systems that interact only via stable mass transfer (no common envelopes). Channels III and IV consist in systems that experience at least one common envelope before the formation of the first BH. The only difference between them is that one of the two stars retains a fraction of its H-rich envelope until the formation of the first BH in channel III, while both stars have lost their envelope by the formation of the first BH in channel IV.

**Figure 11**

Figures 11 and 12 show that this trend is an effect of delay time: the majority of the unequal mass BBHs come from channel II and III. BBHs with low-mass secondary BHs have longer delay times in both channel II and III.

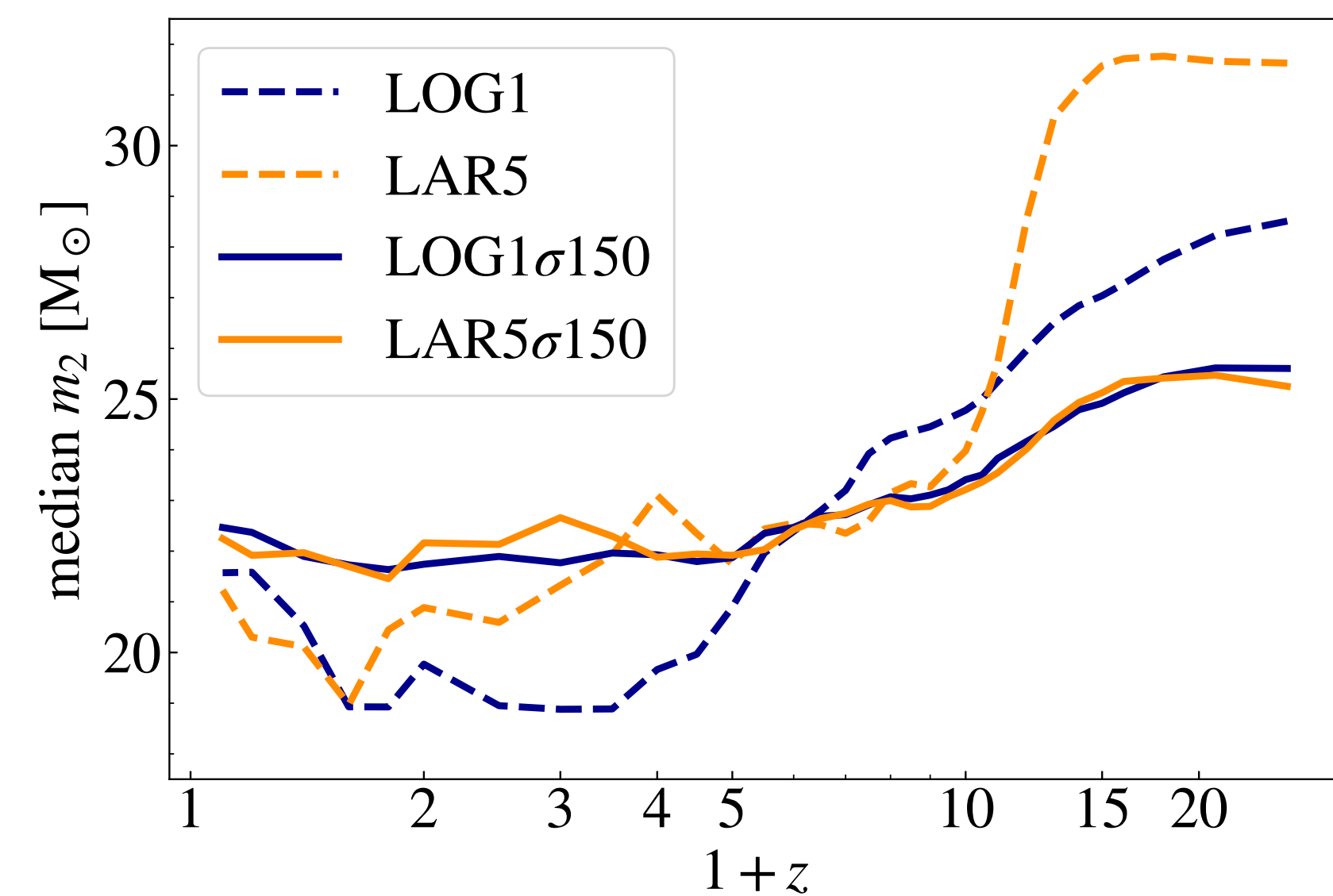
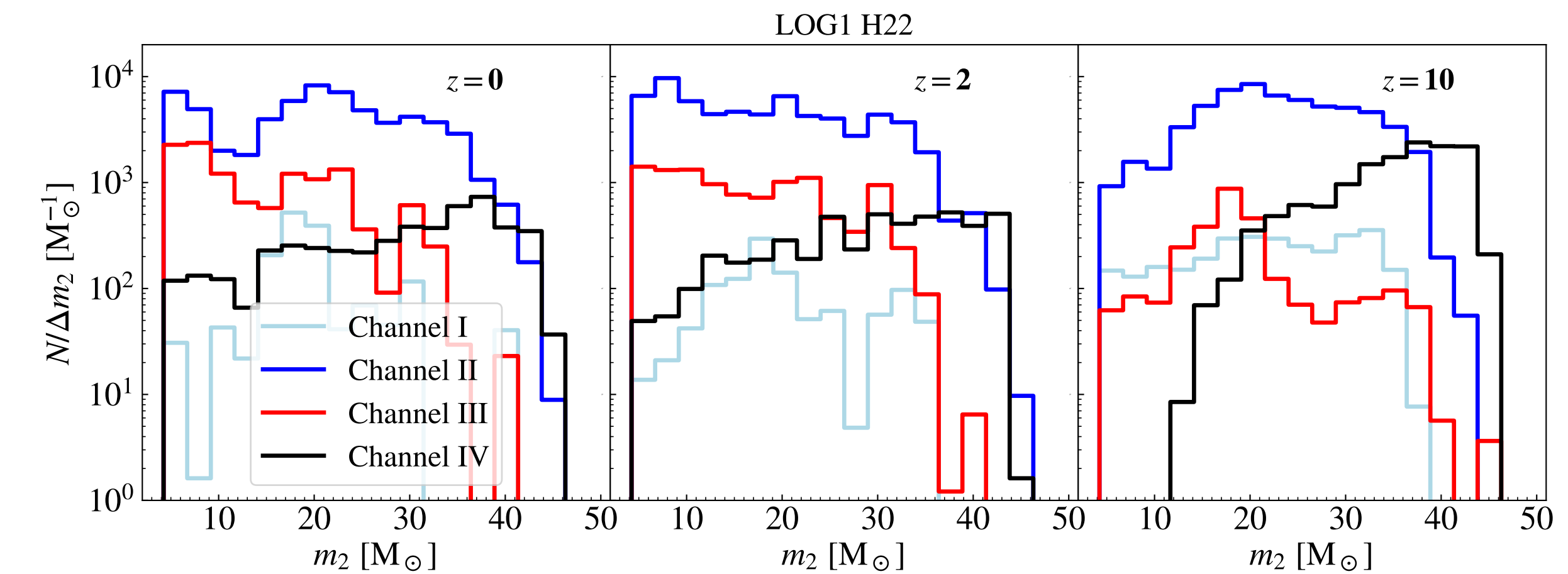
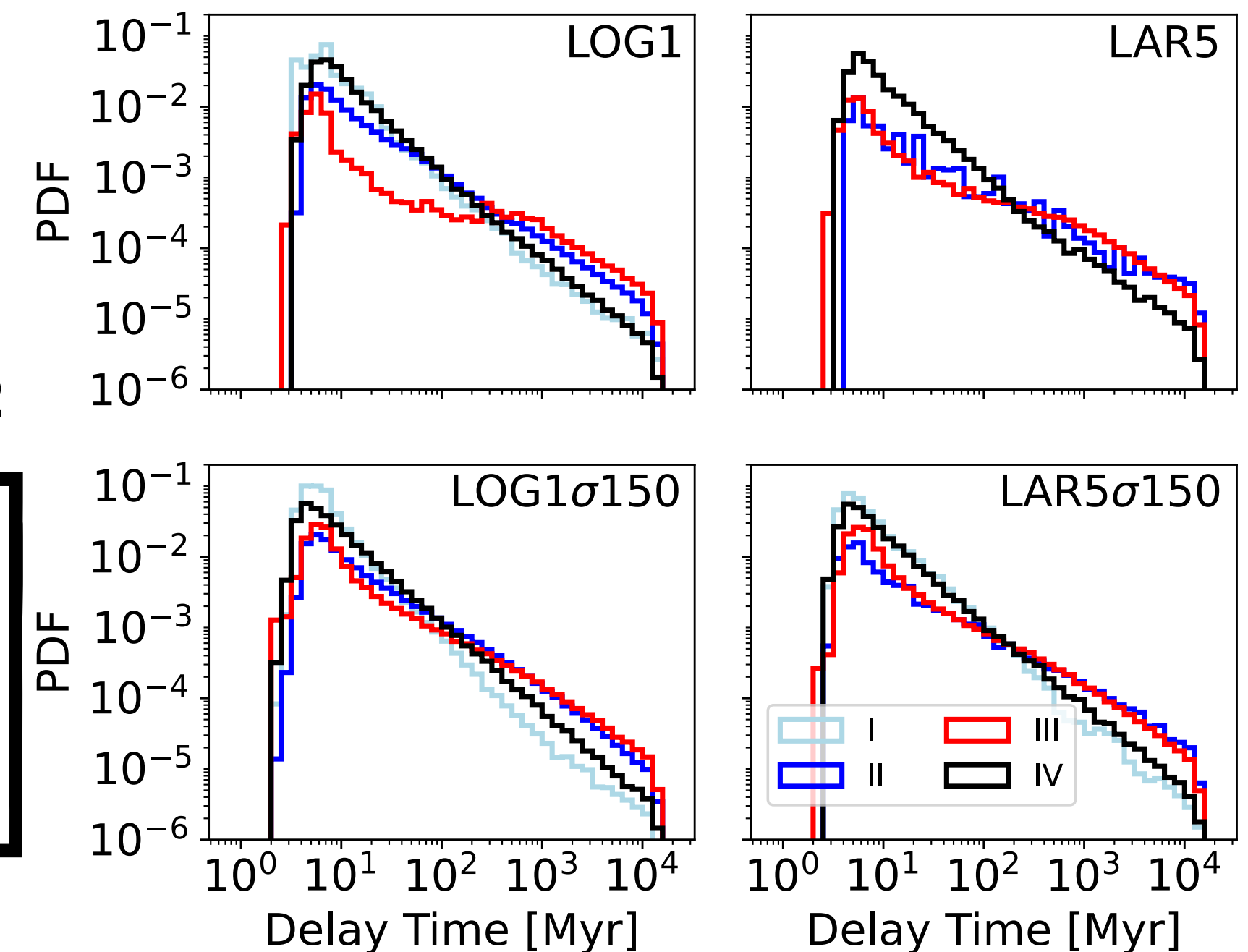


**Figure 12**

This effect is mitigated if we assume a natal kick model that does not depend on properties of the systems



# detection rate

$$\mathcal{R}_{\text{det}} = \int \frac{d^2\mathcal{R}(m_1, m_2, z)}{dm_1 dm_2} \frac{1}{(1+z)} \frac{dV_c}{dz} p_{\text{det}}(m_1, m_2, z) dm_1 dm_2 dz.$$

$$\frac{d^2\mathcal{R}(m_1, m_2, z)}{dm_1 dm_2} = \mathcal{R}(z) p(m_1, m_2 | z).$$

$$\rho = \rho_{\text{opt}} \sqrt{\omega_0^2 + \omega_1^2 + \omega_2^2}$$

$$\rho_{\text{opt}}^2 = 4 \int_{f_{\text{low}}}^{f_{\text{high}}} df \frac{|\tilde{h}(f)|^2}{S_n(f)}$$